*Journal of Earth Science*, *Vol. 30*, *No. 1*, *p. 20–36*, *February 2019* *ISSN 1674-487X*
*Printed in China*
https://doi.org/10.1007/s12583-018-0862-9

# Petrogenesis of the Payangazu Complex in Southern Mandalay, Central Myanmar and Its Tectonic Implications

**Kaixuan Li**[1, 2], **Huaying Liang**[*1], **Zhiwei Bao**[1], **Wenting Huang**[1], **Jian Zhang**[1, 2], **Long Ren**[1, 2]

1. *Key Laboratory of Mineralogy and Metallogeny*, *Guangzhou Institute of Geochemistry*, *Chinese Academy of Sciences*, *Guangzhou* 510640, *China*
2. *University of Chinese Academy of Sciences*, *Beijing* 100049, *China*

Kaixuan Li: https://orcid.org/0000-0001-7136-6948; Huaying Liang: https://orcid.org/0000-0001-9195-4923

**ABSTRACT: The Payangazu complex in the central Myanmar is composed mainly of quartz diorite, granodiorite, and some synplutonic mafic dikes. The quartz diorite and granodiorite have zircon U-Pb ages of 130.5±4.0 (MSWD=3.5) and 118.4±2.5 Ma (MSWD=2.4), respectively. Rock samples of the quartz diorite and granodiorite are metaluminous, enriched in large-ion lithophile elements like LREE, Rb, Th, and U, and depleted in high field-strength elements such as HREE, Nb, Ta, P, and Ti, indicative of arc-type magmatic affinities. Whole rock samples of the quartz diorite have $\varepsilon_{Hf}(t)$ value of +0.6, initial $^{87}Sr/^{86}Sr$ ratios of 0.708 6 to 0.710 0, and $\varepsilon_{Nd}(t)$ values of -4.8 to -4.9; whereas rocks of the granodiorite are relatively isotopically enriched, with $\varepsilon_{Hf}(t)$ values of -5.1 to -7.2, initial $^{87}Sr/^{86}Sr$ ratios of 0.711 7 to 0.711 8, and $\varepsilon_{Nd}(t)$ values of -8.7 to -8.8. The isotopic data together with the high $Mg^{\#}$ (both the quartz diorite and granodiorite have $Mg^{\#}$ values of >40) suggest a strong involvement of mantle materials in the genesis of the parent magmas. The possible petrogenetic process may be that the ascending of melts from partial melting of metasomatized mantle wedge triggered by dehydration of subducted slab resulted in partial melting of the lower crust and mixed with the latter. These Early Cretaceous intrusions from the complex are older than those found in the eastern Wuntho-Popa arc in western Myanmar, eastern Himalaya, and western Yunnan which are interpreted to be related to the Neo-Tethyan subduction, and have $\varepsilon_{Nd}(t)$, $\varepsilon_{Hf}(t)$ values lower than the latter. On the contrary, the ages and geochemical characteristics of the Payangazu complex are consistent with some of the intrusions in the northern magmatic belt in Tibet, eastern Himalaya, and western Yunnan which are believed to be associated with the subduction of the Bangong-Nujiang Ocean crust. Thus, we propose that the Early Cretaceous intrusions in the central Myanmar are most likely related to the southward subduction of an ocean slab that was possibly an extension of the Bangong-Nujiang Ocean.**

**KEY WORDS: central Myanmar, zircon U-Pb age, isotope, Early Cretaceous subduction.**

## 0 INTRODUCTION

Myanmar is tectonically located in the eastern section of the Tethyan tectonic system. The magmatic and tectonic activities in Myanmar are related to different stage subductions of the oceanic slabs and the subsequent collision between continents (Huangfu et al., 2016; Zaw et al., 2014; Metcalfe, 2013; Curray, 2005). These include the slab subductions of the Neo-Tethys and the Paleo-Tethys, and continent-continent collision subsequent to the closure of the Paleo-Tethyan Ocean. In addition, in central Myanmar, an ocean basin was suggested to have existed on the east of the Sagaing fault based on evidences from geochronology and sequence stratigraphy (Prosanta et al., 2017; Mitchell et al., 2012, 2007; Wang et al., 2012; Mitchell, 1993). However, petrogenetic and geochronological investigations on magmatic rocks in central Myanmar are rare whilst previous studies in the region are mostly focused on the metamorphic events of the well-known Mogok metamorphic belt and northern Myanmar because they host plentiful valuable jade and gem deposits (Yonemura et al., 2013; Waltham, 2010; Mitchell et al., 2007; Searle et al., 2007; Barley et al., 2003; Goffé et al., 2002; Bertrand et al., 2001).

A well exposed intrusive complex occurring near the town of Payangazu, in central Myanmar, provides an excellent locus to probe the magmatic origin and tectonic evolution of the region. This complex previously was regarded as diorite with reported age of 131 Ma (Chen et al., 2016) or granodiorite with reported ages of 128 Ma (Mitchell et al., 2012) and 121 Ma (Barley et al., 2003). These petrological inconformity and chronological discrepancy are vary confusing. Besides, their geochemical characteristics of the complex are still unclear. Thus, more detailed chronological results and geochemical data of the intrusions are needed to constrain their petrogenesis and possible tectonic setting.

In this paper, we report precise zircon U-Pb ages and bulk-rock major, trace elements and Sr-Nd-Hf isotopic results

*Corresponding author: lianghy@gig.ac.cn


Manuscript received May 18, 2018.
Manuscript accepted November 3, 2018.

Li, K. X., Liang, H. Y., Bao, Z. W., et al., 2019. Petrogenesis of the Payangazu Complex in Southern Mandalay, Central Myanmar and Its Tectonic Implications. *Journal of Earth Science*, 30(1): 20–36. https://doi.org/10.1007/s12583-018-0862-9. http://en.earth-science.net

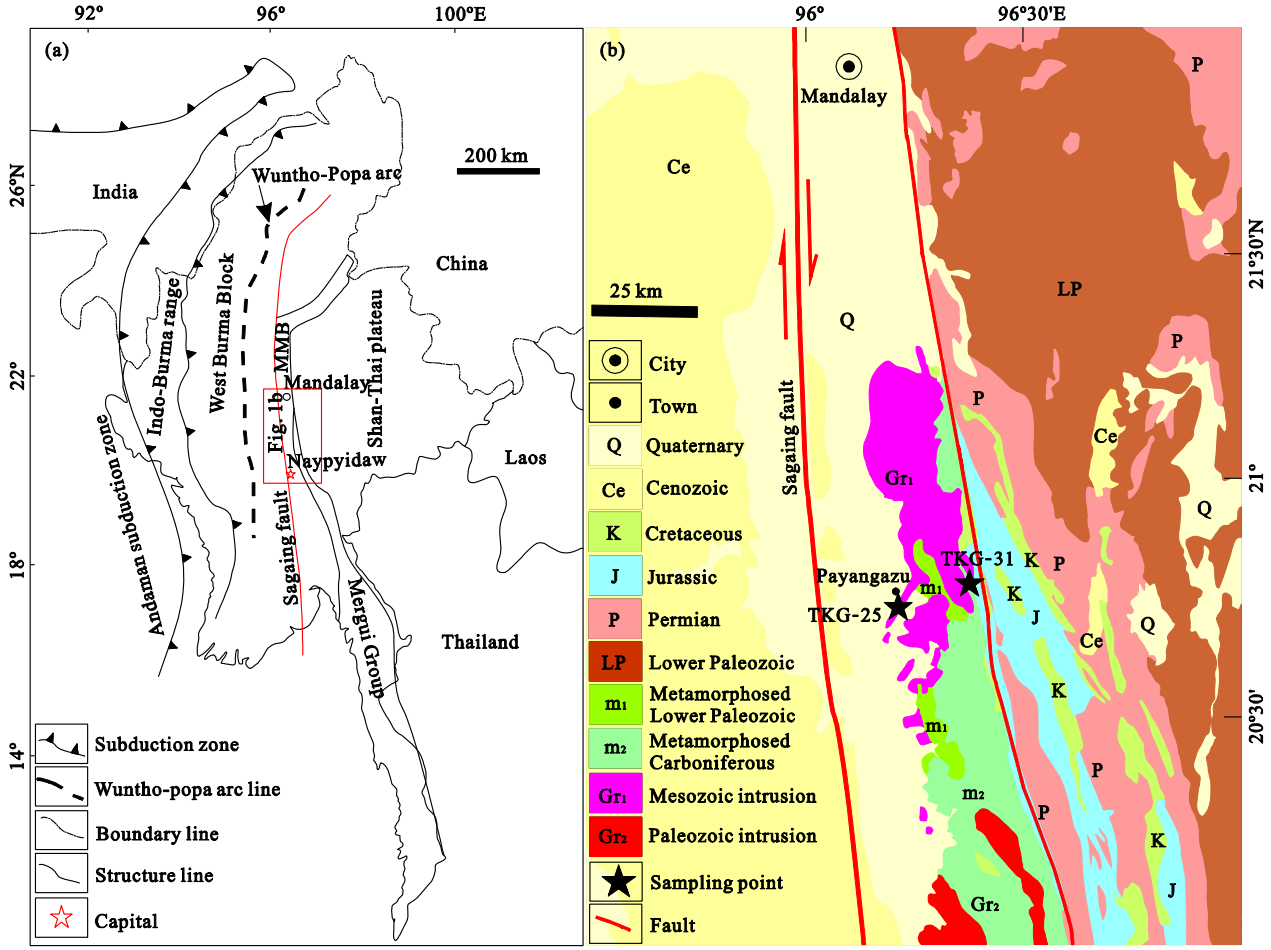


**Figure 1.** (a) Geological map of study area; (b) tectonic outlines of Myanmar. MMB. Mogok metamorphic belt.

of the main rock types from the complex, and discuss their petrogenesis and possible tectonic setting.

## 1 GEOLOGICAL BACKGROUND

### 1.1 Tectonic Zones in Myanmar

Myanmar could be divided into three parts from the west to the east: the Indo-Burma range, the West Burma Block and the Shan-Thai Block (Fig. 1a).

The Indo-Burma range consists mainly of the Late Cretaceous–Paleogene strata and the overlying Cenozoic sediments. Its west boundary is the Andaman subduction zone. This presently active subduction zone extends northward through the Himalayan Syntaxis into India where it transformed into a northward thrust nappe structure. The east boundary is an Early Jurassic ophiolite zone which was regarded as extension of the Yarlung Tsangpo suture zone and was offset by the eastern Himalayan Syntaxis at the north part of Myanmar (Mitchell, 1993). This suture zone represents the subduction of the Neo-Tethyan Ocean and along which ultramafic rocks, pillow basalts, and cherts distribute intermittently.

The West Burma Block situates in-between the ophiolite zone and the Sagaing fault, and it has stratigraphic units similar to those of the Indo-Burma range. The Sagaing fault, an important dextral strike-slip fault accommodating the collision of India and Southeast Asian Plate in the Eocene, is about 1 200 km long and terminates near the eastern Himalayan Syntaxis (Maurin et al., 2010; Curray, 2005). In the central part of the block, there is a north-south magmatic belt called Wuntho-Popa magmatic arc which consists mainly of the Late Cretaceous granodiorite batholith, some small Late Cretaceous to Early Tertiary calc-alkaline intrusions and the Late Cretaceous to Quaternary volcanic strata.

The Shan-Thai Block in the east part of Myanmar is located to the east of the Sagaing fault and west of the Bentong-Chiang Rai suture. The suture is characterized by remnants of the Paleo-Tethys Ocean subduction and the subsequent collision between the Shan-Thai Block and Indochina Block in the Late Triassic (Metcalfe, 1988; Mitchell, 1977). The Shan-Thai Block together with Malay Peninsula, the eastern Sumatra, and the Baoshan Block in Yunnan Province of China was termed as the Sibumasu Block (Metcalfe, 1988). The strata of this block are mainly composed of the Cambrian to Triassic strata with overlying Upper Jurassic–Lower Cretaceous sediments (Barber et al., 2005; Mitchell, 1992). The Shan-Thai Block could be subdivided as Shan Plateau and Shan scarps. The Shan scarps on the east margin of the Shan-Thai Block consist of two stratigraphic units. One is the well-known Mogok metamorphic belt which stretches embowed and bends towards the eastern Himalayan Syntaxis in the north part of Myanmar. The other unit is the Mergui Group, which distributes in the east part of the Mogok metamorphic belt and absent in the north part of Myanmar. In Shan scarps, a Mogok-Mandalay-Mergui magmat-

ic belt with granitoids of the Late Cretaceous and Paleocene–Eocene was identified (Gardiner et al., 2015; Mitchell et al., 2012; Barley et al., 2003). The Shan Plateau, making up the major part of Shan-Thai Block, is separated from the Shan scarps by an east-dipping fault and an ocean regarded as the extension of the Nujiang-Luxi Ocean situated in-between the Tengchong and Baoshan blocks in Southwest China (Mitchell et al., 2012, 2007; Wang et al., 2012; Mitchell, 1993).

### 1.2 The Intrusive Complex in Central Myanmar

The Payangazu complex is located about 130 km south of Mandalay (Fig. 1b). The complex consists of largely granodiorite in the east part and minor quartz diorite in the west part, and some synplutonic mafic dikes. The complex intruded the Mogok metamorphic belt and the Mergui Group. The biotite and garnet bearing augen gneiss, schists, and minor marble and pegmatite veins, which are believed to be the metamorphosed Lower Paleozoic–Mesozoic strata of the Mogok metamorphic belt, occur at the west side of the complex; whereas the mica schists of the Mogok metamorphic belt and the overlying diamictites of the Mergui Group occur at the east side of the complex. Far to the east, the diamictites are in turn overlain by the Late Jurassic limestone and clastic rocks, and some volcanic and pyroclastic rocks. Hornfels were observed near the contact of the intrusions and the diamictites.

The granodiorite has medium-coarse grained texture and composes of about 50%–60% plagioclase, 10%–15% K-feldspar, 5%–10% hornblende, 20%–25% quartz, 5%–10% biotite, and accessory minerals including titanite, apatite, zircon, and magnetite (Fig. 2). The quartz diorite is coarse-grained with plagioclase content of 50%–60%, K-feldspar content of 5%–10%, hornblende content of 10%–20%, biotite content of 5%–10% and quartz content of 5%–10%. The intrusive mafic dikes extend in north-south direction with width ranging from 40 cm to 2 m and length of tens to hundreds meters.

## 2 METHODS

Five least altered samples of each rock types were selected for major and trace elements analyses. They were crushed to grains of about 2–5 mm, leached by 3% HCl solution, then rinsed by deionized water. After dried at temperature of 100 ºC, the samples were ground to less 200 meshes for bulk major, trace element and isotopic analyses. Zircon crystals from the quartz diorite (TGK-25) and granodiorite (TKG-31) were separated for U-Pb geochronological study. All the analyses were carried out at the National Key Laboratory of Isotope Geochemistry, Guangzhou Institute of Geochemistry, Chinese Academy of Sciences.

### 2.1 Major and Trace Element Analyses

The major elements contents of bulk rock samples were analyzed by using X-ray fluorescent spectrometry following procedures described by Goto and Tatsumi (1996). The analytical precision was better than 5%. The loss on ignition (LOI) was calculated by weighing the difference before and after the burning at temperature of about 900 ºC. In order to proceed

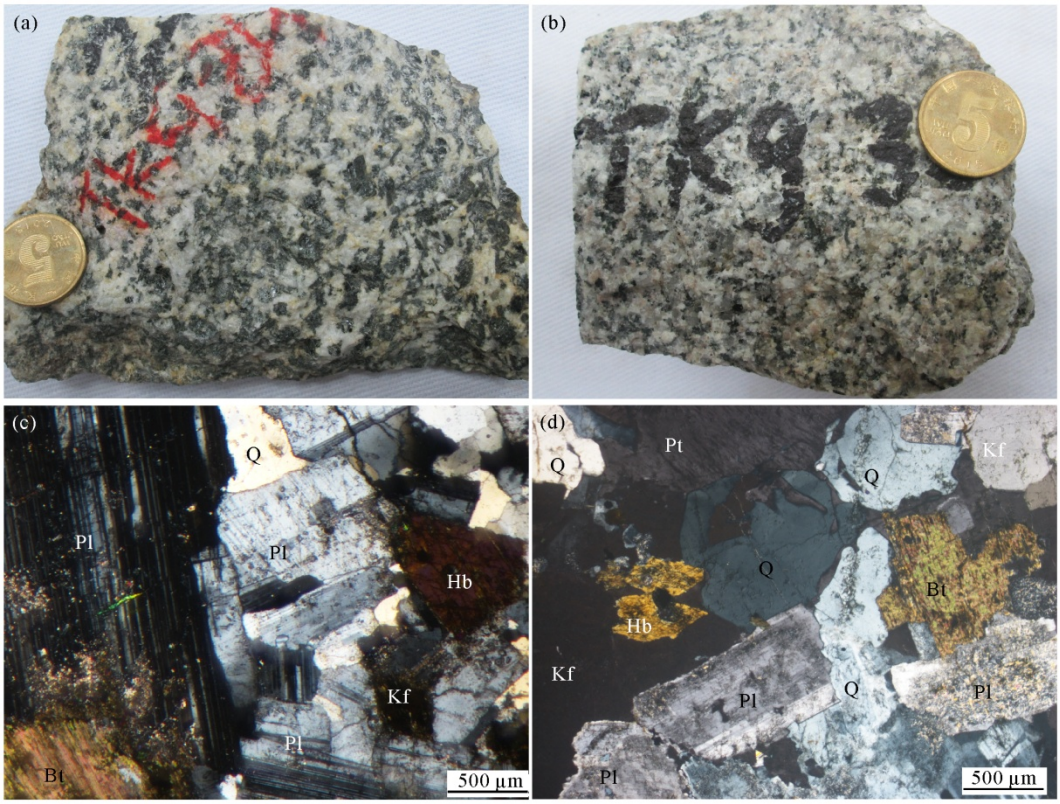


**Figure 2.** Hand specimen photos and photomicrographs of the diorite and granodiorite from the central Myanmar. (a) Diorite; (b) granodiorite; (c) photo showing mineral assemblage of diorite under perpendicular polarized light; (d) photo showing mineral assemblage of granodiorite under perpendicular polarized light. Q. Quartz; Kf. K-feldspar; Pl. plagioclase; Pt. perthite; Hb. hornblende; Bt. biotite.

trace element analysis, about 50 mg powdered samples were dissolved in Teflon bombs using mixed acids of HF and $HNO_3$ at about 200 ºC for two days. After the dissolution, the generated sample solutions were transferred into test tubes and diluted for analysis. The trace element concentrations of the rocks were determined by using inductively coupled plasma mass spectrometry method on a PerkinElmer Elan, 9000, details of the procedures are similar to those described by Liu et al. (1996). Rh was used as an internal standard to monitor signal drift during the analysis. The analytical precision of which is better than 10%.

### 2.2 Whole-Rock Sr-Nd-Hf Isotopic Analysis

Whole-rock Sr-Nd-Hf isotopic compositions were measured on a Neptune Plus multi-collector mass spectrometer of Isoprobe. The analytical procedures for the Sr, Nd isotopic compositions are similar to those described by Yang et al. (2011). The mass fractionation of Sr and Nd were corrected by using the values of $^{86}Sr/^{88}Sr=0.119\ 4$ and $^{146}Nd/^{144}Nd=0.721\ 9$ respectively. The analytical standards used during the measurement were the NIST SRM 987 with $^{87}Sr/^{86}Sr=0.710\ 290\pm 0.000\ 014$ ($2\sigma$) and the Shin Etsu JNdi-1 with $^{143}Nd/^{144}Nd=0.512\ 094\pm0.000\ 008$ ($2\sigma$). The analytical procedure for Hf isotope follows Li et al. (2006). Briefly, 0.5 g powdered rock samples was mixed with 1.0 g $Li_2B_4O_7$, and put into high-frequency furnace and melted in Pt crucibles at 1 250 ºC for 15 min. And then the samples were crushed and dissolved in the 2 mol/L HCl. The mass fractionation correction of Hf was based on $^{179}Hf/^{177}Hf=0.732\ 5$. During the analysis, the values of $^{176}Lu/^{175}Lu=0.026\ 549$ and $^{176}Yb/^{173}Yb=0.786\ 96$ were used to calculate the concentrations of $^{176}Lu$ and $^{176}Yb$, and then the influences of them were deducted.

### 2.3 Zircon U-Pb Chronology

Zircon crystals from the quartz diorite and granodiorite were separated using conventional heavy liquid and magnetic separation techniques, and handpicked under a binocular microscope. The zircon grains were mounted on a transparent epoxy resin disk and polished near the core to expose the internal structures. Cathodoluminescence (CL) images and microscopic observation were made to study the internal structure.

U-Pb dating of zircon was conducted on inductively coupled plasma mass spectrometry equipped with a laser ablation system (LA-ICP-MS). The epoxy resin disks with embedded zircons were placed in a special sample cell which flushed with He and Ar. The laser used for ablation was a pulsed resonetic 193 nm ArF excimer laser with constant energy of 80 mJ and repetition rate of 8 Hz. The diameter of ablating spot was 31 μm. The ablated aerosol was delivered to an Agilent 7500a ICP-MS by carrier gas of He and detected there (Tu et al., 2011). Standard of zircon 91500 was used as an external standard during U-Pb dating (Black et al., 2003; Wiedenbeck et al., 1995), and analyses of the standard were conducted twice for every five analyses of the samples. Off-line inspection, integration of background and analytical signals, time-drift correction and quantitative calibration for U-Pb dating were performed by using ICPMSDataCal (Liu et al., 2008). Concordia diagrams and weighted mean values calculation were made by Isoplot/Ex Version 3.0 (Ludwig, 2003).

## 3 RESULTS

### 3.1 Whole-Rock Major and Trace Elements

The major and trace elemental concentrations of the quartz diorite and granodiorite from the Payangazu complex are listed in Table 1. The quartz diorite has $SiO_2$ of 61.1 wt.%–63.2 wt.%, $Na_2O$ of 3.18 wt.%–4.20 wt.%, $K_2O$ of 1.56 wt.%–2.47 wt.%, $Al_2O_3$ of 15.7 wt.%–17.1 wt.%. The granodiorite has higher $SiO_2$ (65.7 wt.%–66.8 wt.%) and $K_2O$ (3.20 wt.%–3.80 wt.%) contents and relative lower $Al_2O_3$ (14.5 wt.%–15.3 wt.%) and $Na_2O$ (2.93 wt.%–3.18 wt.%). On the TAS diagram (Fig. 3a), the quartz diorite falls into the field of diorite and the granodiorite fall into the field of granodiorite, which are consistent with their mineral compositions. Both the quartz diorite and the granodiorite are largely metaluminous and belong to calc-alkaline and high-K calc-alkaline series, respectively (Figs. 3b–3c).

The two type rocks have similar trace elements and REE (rare earth element) patterns (Fig. 4). Rare earth element (REE) concentrations of the quartz diorite and granodiorite vary in ranges of 96.7 ppm–160.0 ppm and 161.0 ppm–271.1 ppm, respectively. As shown in the chondrite normalized REE patterns (Fig. 4a), both the quartz diorite and the granodiorite have moderate negative Eu anomalies, highly fractionated light rare element and weak- or non-fractionated heavy rare earth element, which are characterized by high $(La/Yb)_N$ ratios of 3.64–8.78 and 7.64–17.28, respectively. The primitive mantle normalized trace element spider diagrams of the rocks exhibit arc-type signatures such as enriched large ion lithophile elements (e.g., Rb, Th, U) and depleted high field strength elements (HFSE) (e.g., Nb, Ta, P, Ti) (Fig. 4b).

### 3.2 Zircon U-Pb Ages

Zircon grains from the quartz diorite (sample TKG-25) and granodiorite (sample TKG-31) are euhedral crystals with length of 150–200 m, width of 50–120 m and length of 100–200 m, width of 50–120 m, respectively. On the cathodoluminescence images (Fig. 5), all the zircon crystals show clear oscillatory zoning, indicative of a magmatic origin (Hoskin, 2003).

The analytical results for zircon grains from the quartz diorite (TKG-25) are listed in Table 2. The zircons have U and Th concentrations of 145 ppm–285 ppm and 114 ppm–340 ppm, respectively, with U/Th ratios of 0.63–1.19. Removing those with concordance of less than 90%, 14 qualified data set of the 20 tests yielded a weighed mean $^{206}Pb/^{238}U$ age of 130.5±4.0 Ma ($1\sigma$, MSWD=3.5) (Fig. 6a). U-Pb isotopic results for zircon grains from the granodiorite (TKG-31) are listed in Table 3. The zircon crystals have U and Th concentrations in ranges of 114 ppm–681 ppm and 104 ppm–690 ppm, respectively, with U/Th ratios of 0.61–1.50. Removing those with concordance of less than 90%, 15 of the 20 tests yielded a weighed mean $^{206}Pb/^{238}U$ age of 118.4±2.5 Ma ($1\sigma$, MSWD=2.4) (Fig. 6b).

### 3.3 Whole-Rock Sr-Nd-Hf Isotopes

The Sr-Nd-Hf isotopic compositions for the quartz diorite and granodiorite are listed in Table 4 and Table 5. The Rb, Sr,

**Table 1** Major (wt.%) and trace element (ppm) concentrations of the diorite and granodiorite intrusions in the central Myanmar

| Rock type | Diorite | | | | | Granodiorite | | | | |
|---|---|---|---|---|---|---|---|---|---|---|
| Sample No. | TKG-24 | TKG-25 | TKG-26 | TKG-27 | TKG-28 | TKG-29 | TKG-30 | TKG-31 | TKG-32 | TKG-33 |
| $SiO_2$ | 61.4 | 61.2 | 62.5 | 63.2 | 61.1 | 65.7 | 66.8 | 66.8 | 66.4 | 66.5 |
| $TiO_2$ | 0.66 | 0.65 | 0.58 | 0.64 | 0.66 | 0.57 | 0.51 | 0.51 | 0.52 | 0.54 |
| $Al_2O_3$ | 17.1 | 16.8 | 16.6 | 15.7 | 16.8 | 14.5 | 14.9 | 15.1 | 15.3 | 15.3 |
| $Fe_2O_3^T$ | 5.84 | 6.09 | 5.16 | 6.17 | 6.28 | 5.36 | 4.45 | 4.42 | 4.43 | 4.46 |
| MnO | 0.11 | 0.10 | 0.10 | 0.10 | 0.11 | 0.10 | 0.08 | 0.08 | 0.10 | 0.10 |
| MgO | 2.66 | 2.78 | 2.63 | 2.75 | 2.82 | 2.00 | 1.59 | 1.64 | 1.68 | 1.67 |
| CaO | 5.38 | 5.74 | 3.86 | 4.85 | 5.42 | 3.76 | 3.58 | 3.78 | 3.79 | 3.75 |
| $Na_2O$ | 3.39 | 3.66 | 4.20 | 3.18 | 3.44 | 2.97 | 3.06 | 3.18 | 2.93 | 2.96 |
| $K_2O$ | 2.06 | 1.56 | 1.68 | 2.47 | 2.30 | 3.71 | 3.59 | 3.20 | 3.80 | 3.71 |
| $P_2O_5$ | 0.17 | 0.14 | 0.12 | 0.13 | 0.14 | 0.15 | 0.12 | 0.12 | 0.17 | 0.13 |
| LOI | 1.15 | 0.74 | 2.42 | 0.74 | 0.95 | 0.82 | 0.70 | 1.10 | 0.86 | 0.89 |
| Total | 99.9 | 99.4 | 99.8 | 100 | 100 | 99.7 | 99.4 | 99.9 | 100 | 100 |
| A/NK | 2.19 | 2.17 | 1.90 | 1.98 | 2.06 | 1.63 | 1.67 | 1.73 | 1.71 | 1.72 |
| A/CNK | 0.97 | 0.92 | 1.05 | 0.94 | 0.93 | 0.92 | 0.97 | 0.97 | 0.96 | 0.97 |
| $Mg^{\#}$ | 47.4 | 47.5 | 50.2 | 46.9 | 47.1 | 42.5 | 41.4 | 42.4 | 42.8 | 42.5 |
| Sc | 14.1 | 13.4 | 12.5 | 14.7 | 13.9 | 12.6 | 11.4 | 14.2 | 10.4 | 10.4 |
| Co | 16.4 | 15.0 | 13.0 | 14.1 | 15.4 | 11.0 | 10.7 | 10.4 | 7.90 | 8.80 |
| Ni | 35.8 | 15.2 | 13.9 | 15.5 | 15.4 | 32.0 | 31.4 | 8.80 | 7.10 | 7.70 |
| Ga | 18.7 | 18.5 | 17.8 | 17.9 | 18.6 | 18.7 | 19.6 | 18.4 | 17.9 | 18.3 |
| Rb | 82.6 | 80.6 | 58.1 | 100 | 93.7 | 167 | 171 | 178 | 171 | 164 |
| Sr | 309 | 329 | 288 | 279 | 323 | 300 | 291 | 276 | 297 | 300 |
| Y | 26.5 | 21.3 | 20.1 | 23.1 | 21.5 | 30.3 | 27.6 | 23.7 | 23.8 | 26.1 |
| Zr | 124 | 195 | 141 | 161 | 208 | 182 | 213 | 198 | 179 | 202 |
| Nb | 8.47 | 8.50 | 8.40 | 8.80 | 8.80 | 13.9 | 13.6 | 13.2 | 13.2 | 14.1 |
| Ba | 413 | 322 | 394 | 498 | 576 | 583 | 499 | 596 | 553 | 438 |
| La | 32.6 | 15.2 | 28.9 | 35.6 | 30.0 | 32.3 | 39.7 | 66.5 | 49.5 | 38.9 |
| Ce | 61.4 | 35.8 | 55.2 | 68.5 | 58.8 | 65.8 | 76.1 | 125 | 93.1 | 78.2 |
| Pr | 6.57 | 4.11 | 5.30 | 6.51 | 5.97 | 7.57 | 8.22 | 11.9 | 9.14 | 8.07 |
| Nd | 24.4 | 18.8 | 20.9 | 25.3 | 24.2 | 29.2 | 30.1 | 42.5 | 33.9 | 31.3 |
| Sm | 4.57 | 4.15 | 3.98 | 4.73 | 4.68 | 5.89 | 5.47 | 6.15 | 5.62 | 5.70 |
| Eu | 1.06 | 1.11 | 1.02 | 1.15 | 1.20 | 1.18 | 1.10 | 1.18 | 1.20 | 1.17 |
| Gd | 4.40 | 4.56 | 3.96 | 4.74 | 4.69 | 5.23 | 4.79 | 5.10 | 4.82 | 5.12 |
| Tb | 0.71 | 0.77 | 0.66 | 0.77 | 0.77 | 0.85 | 0.75 | 0.79 | 0.77 | 0.88 |
| Dy | 4.42 | 4.75 | 4.17 | 4.88 | 4.83 | 5.24 | 4.55 | 4.59 | 4.61 | 4.91 |
| Ho | 0.93 | 0.98 | 0.87 | 1.03 | 1.00 | 1.05 | 0.94 | 0.89 | 0.91 | 1.03 |
| Er | 2.59 | 2.84 | 2.48 | 3.03 | 2.97 | 2.90 | 2.64 | 2.61 | 2.73 | 3.07 |
| Tm | 0.40 | 0.43 | 0.36 | 0.44 | 0.42 | 0.45 | 0.41 | 0.39 | 0.39 | 0.43 |
| Yb | 2.51 | 2.82 | 2.43 | 2.88 | 2.80 | 2.86 | 2.70 | 2.60 | 2.64 | 2.90 |
| Lu | 0.38 | 0.40 | 0.39 | 0.45 | 0.42 | 0.42 | 0.41 | 0.39 | 0.39 | 0.43 |
| Hf | 3.53 | 5.50 | 4.00 | 4.60 | 5.70 | 5.00 | 5.66 | 5.70 | 5.10 | 5.90 |
| Ta | 0.64 | 0.70 | 0.80 | 0.80 | 0.70 | 1.18 | 1.16 | 1.00 | 1.20 | 1.40 |
| Th | 13.1 | 5.59 | 12.2 | 15.4 | 11.9 | 22.0 | 40.3 | 26.9 | 25.8 | 22.5 |
| U | 1.65 | 1.88 | 2.10 | 2.32 | 1.79 | 2.96 | 8.45 | 4.29 | 4.50 | 4.24 |
| δEu | 0.72 | 0.78 | 0.79 | 0.74 | 0.78 | 0.65 | 0.66 | 0.64 | 0.70 | 0.66 |
| ∑REE | 147 | 96.7 | 131 | 160 | 143 | 161 | 178 | 271 | 210 | 182 |
| LR/HR | 7.99 | 4.51 | 7.53 | 7.78 | 6.97 | 7.47 | 9.35 | 14.62 | 11.15 | 8.70 |
| $(La/Sm)_N$ | 4.49 | 2.31 | 4.57 | 4.74 | 4.03 | 3.45 | 4.56 | 6.81 | 5.54 | 4.30 |
| $(Gd/Yb)_N$ | 1.42 | 1.31 | 1.32 | 1.33 | 1.36 | 1.48 | 1.44 | 1.59 | 1.48 | 1.43 |
| $(La/Yb)_N$ | 8.78 | 3.64 | 8.04 | 8.35 | 7.24 | 7.64 | 9.94 | 17.3 | 12.7 | 9.06 |

$Mg^{\#}$=100×molar Mg/(Mg+Fe); $Fe_2O_3^T$ is stand for total iron.

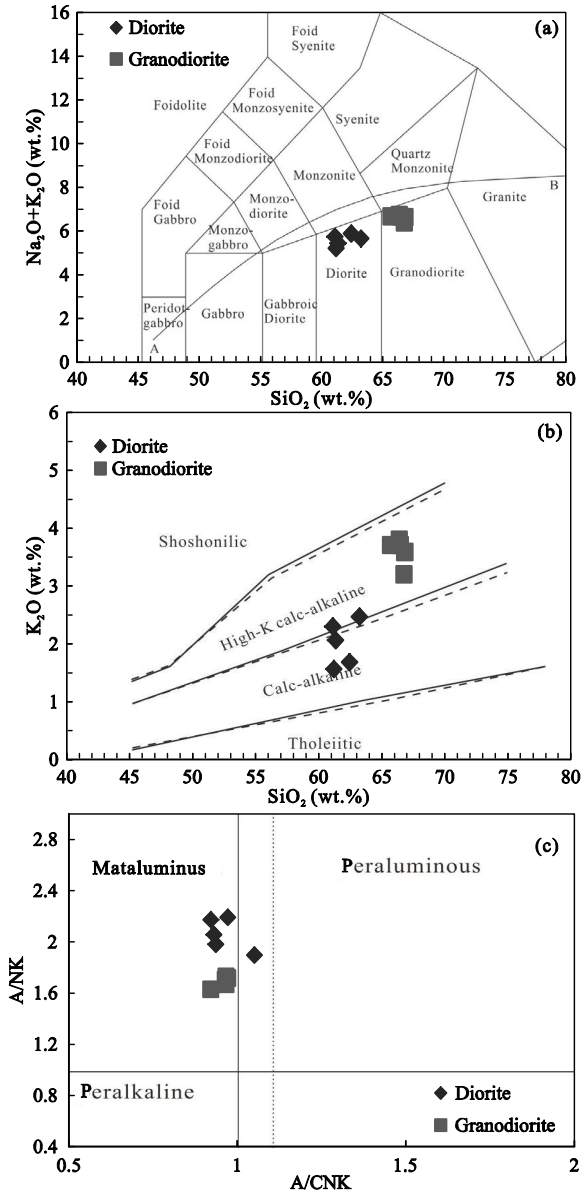


**Figure 3.** (a) TAS diagram (Middlemost, 1994); (b) $K_2O$ vs. $SiO_2$ diagram (Rollinson, 1993; Peccerillo and Taylor 1976); (c) A/NK (molar ratio $Al_2O_3/(Na_2O+K_2O)$) vs. A/CNK (molar ratio $Al_2O_3/(CaO+Na_2O+K_2O)$) diagram (Maniar and Piccoli, 1989).

Sm, Nd, Lu and Hf concentrations of the whole-rock samples in Table 1 and zircon U-Pb ages were used to calculate the initial $^{87}Sr/^{86}Sr$ ratios, $\varepsilon_{Hf}(t)$ and $\varepsilon_{Nd}(t)$ values.

Two quartz diorite samples have initial $^{87}Sr/^{86}Sr$ ratios of 0.708 6 and 0.710 0 and $\varepsilon_{Nd}(t)$ values of -4.8 and -4.9 with the calculated two stage model ages ($T_{DM2}$) of 1 319 and 1 323 Ma. Two granodiorite samples show initial $^{87}Sr/^{86}Sr$ ratios of 0.711 8 and 0.711 7 and $\varepsilon_{Nd}(t)$ values of -8.7 and -8.8 with calculated $T_{MD2}$ of 1 623 and 1 627 Ma. One quartz diorite sample and two granodiorite samples were selected for whole-rock Hf isotopic analysis. The quartz diorite sample has $\varepsilon_{Hf}(t)$ of 0.6 and two stage model age ($T_{MD}^{C}$) of 1 147 Ma the two granodiorite samples have $\varepsilon_{Hf}(t)$ values of -7.2 and -5.1 and $T_{MD}^{C}$ of 1 127 and 1 498 Ma.

## 4 DISCUSSION

### 4.1 Zircon U-Pb Ages of Payangazu Complex

Zircon U-Pb ages of 130.5±4.0 and 118.4±2.5 Ma for the quartz diorite and granodiorite, respectively. Our new data are identical to the previously published ages of 128–131 Ma (Chen et al., 2016; Mitchell et al., 2012) and 121 Ma (Searle et al., 2007) correspondingly within errors. Thus, the complex was emplaced in the Early Cretaceous. However, there is a proximate 10 Ma temporal interval between the two kind rocks and this interval seems too short for magmas to originate in two episodes. The interval may indicate that the magmas originated in one episode and subsequently went through different evolutionary processes and finally emplaced and crystallized in two stages. These Early Cretaceous ages are earlier than those Late Cretaceous to Paleogene magmatic rocks in the west Wuntho-Popa arc (Wang et al., 2014; Mitchell et al., 2012) and the Late Cretaceous granitoids in the southern Myanmar (Jiang et al., 2017; Gardiner et al., 2015; Mitchell et al., 2012). It is interesting to note that the Early Cretaceous magmatism has rarely been reported in other areas of Myanmar, which may imply an unknown or largely ignored tectonic event.

### 4.2 Petrogenesis

#### 4.2.1 Magmatic affinity and significance

Both of the granodiorite and quartz diorite are metaluminous and belong to calc-alkaline to high-K calc-alkaline

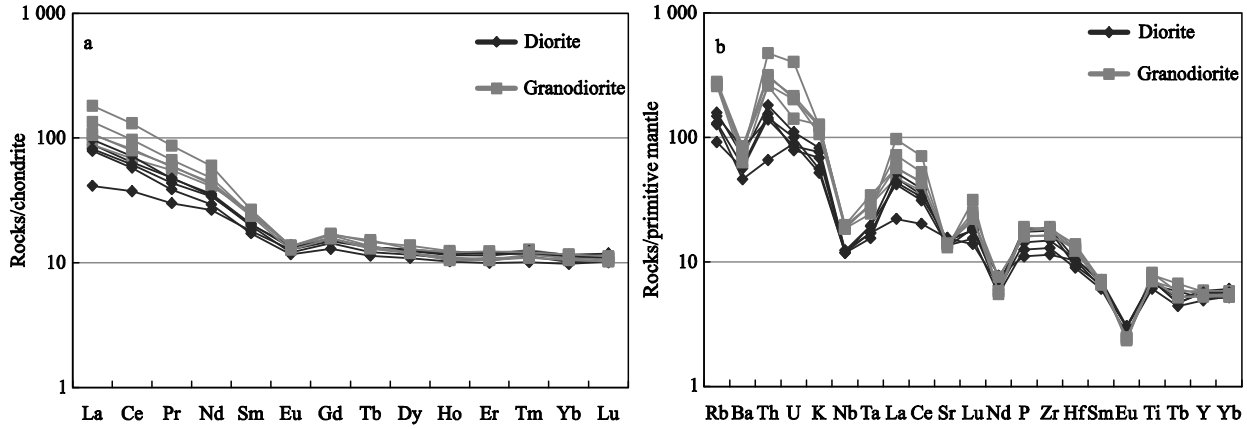


**Figure 4.** Chondrite-normalized rare earth elements and primitive mantle-normalized trace element spiderdiagrams for the diorite and granodiorite. Normalized values of chondrite and primitive mantle are from Sun and McDonough (1989).

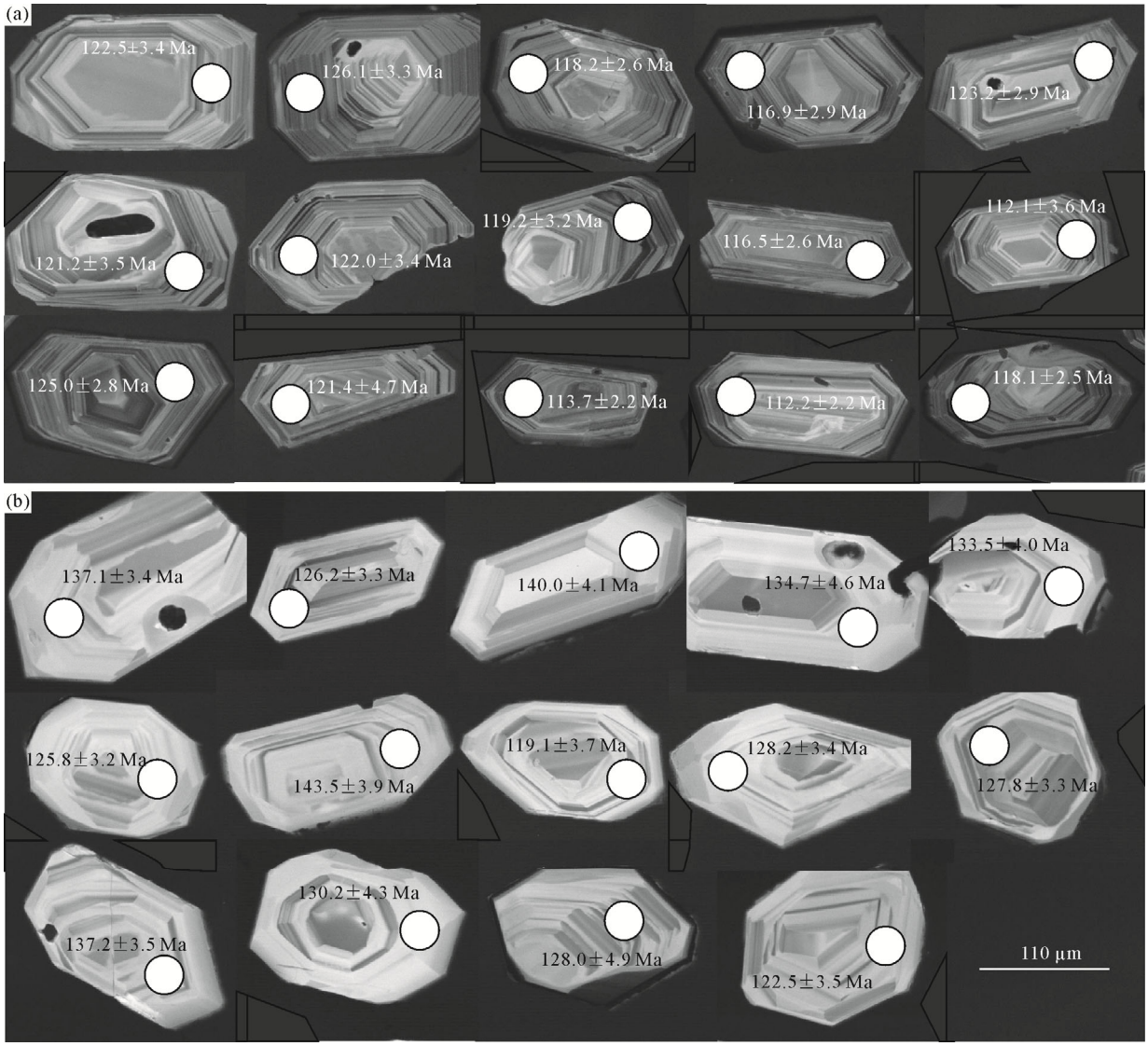


**Figure 5.** The CL images of representative zircons analyzed for in situ ages. Small dots indicate the sites of ablation and the obtained ages were also labelled on the images. (a) Zircons from granodiorite; (b) zircons from diorite.

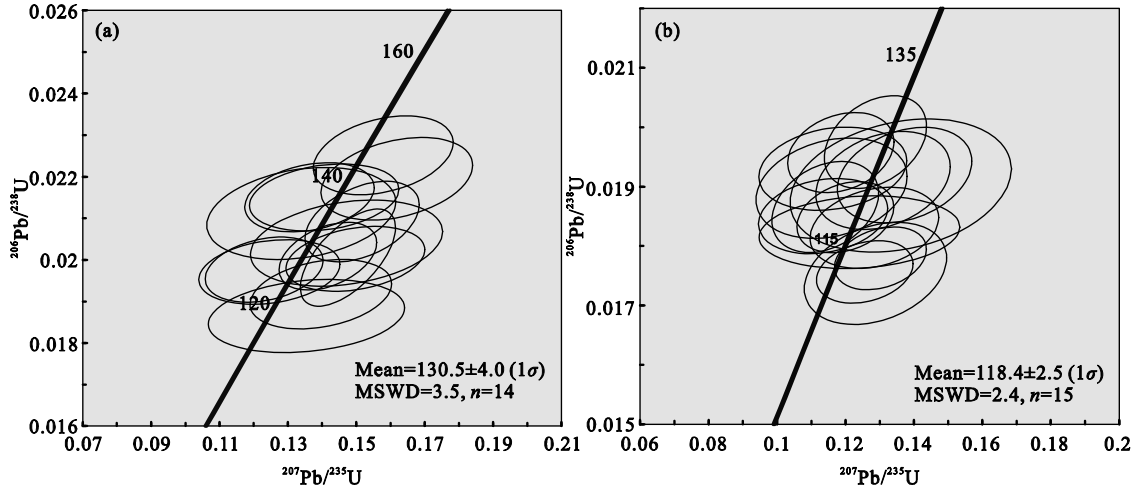


**Figure 6.** U-Pb concordia plots of zircons from the diorite (a) and the granodiorite (b).

**Table 2** U-Pb dating results for zircons from the diorite

| Spot No. | Content (ppm) | | | Th/U | Isotopic ratios | | | | | | Isotopic age (Ma) | | | | | |
|---|---|---|---|---|---|---|---|---|---|---|---|---|---|---|---|---|
| | Pb | Th | U | | $^{207}Pb/^{206}Pb$ | $\pm1\sigma$ | $^{207}Pb/^{235}U$ | $\pm1\sigma$ | $^{206}Pb/^{238}U$ | $\pm1\sigma$ | $^{207}Pb/^{206}Pb$ | $\pm1\sigma$ | $^{207}Pb/^{235}U$ | $\pm1\sigma$ | $^{206}Pb/^{238}U$ | $\pm1\sigma$ |
| TKG-25 | | | | | | | | | | | | | | | | |
| 25-1 | 6.8 | 209 | 227 | 0.92 | 0.049 0 | 0.005 0 | 0.140 6 | 0.014 4 | 0.021 5 | 0.000 5 | 150 | 222 | 134 | 13 | 137 | 3 |
| 25-4 | 5.7 | 185 | 201 | 0.92 | 0.048 4 | 0.005 1 | 0.123 1 | 0.011 4 | 0.019 8 | 0.000 5 | 117 | 233 | 118 | 10 | 126 | 3 |
| 25-5 | 5.5 | 179 | 179 | 1.00 | 0.058 3 | 0.006 1 | 0.161 9 | 0.014 6 | 0.022 0 | 0.000 7 | 539 | 227 | 152 | 13 | 140 | 4 |
| 25-6 | 4.3 | 130 | 152 | 0.86 | 0.047 0 | 0.006 1 | 0.133 9 | 0.018 2 | 0.021 1 | 0.000 7 | 56 | 289 | 128 | 16 | 135 | 5 |
| 25-7 | 5.3 | 167 | 178 | 0.94 | 0.057 0 | 0.006 7 | 0.151 7 | 0.011 0 | 0.020 9 | 0.000 6 | 500 | 261 | 143 | 10 | 133 | 4 |
| 25-8 | 4.2 | 124 | 152 | 0.81 | 0.047 8 | 0.005 6 | 0.124 6 | 0.013 6 | 0.019 7 | 0.000 5 | 100 | 246 | 119 | 12 | 126 | 3 |
| 25-10 | 6.3 | 125 | 198 | 0.63 | 0.052 8 | 0.005 0 | 0.157 9 | 0.013 5 | 0.022 5 | 0.000 6 | 320 | 210 | 149 | 12 | 144 | 4 |
| 25-11 | 4.1 | 124 | 151 | 0.83 | 0.054 5 | 0.007 5 | 0.135 5 | 0.018 9 | 0.018 7 | 0.000 6 | 391 | 308 | 129 | 17 | 119 | 4 |
| 25-12 | 8.6 | 289 | 263 | 1.10 | 0.051 1 | 0.003 6 | 0.141 7 | 0.009 4 | 0.020 1 | 0.000 5 | 256 | 195 | 135 | 8 | 128 | 3 |
| 25-13 | 7.8 | 271 | 253 | 1.07 | 0.055 9 | 0.005 8 | 0.149 7 | 0.013 4 | 0.020 0 | 0.000 5 | 456 | 232 | 142 | 12 | 128 | 3 |
| 25-15 | 9.1 | 340 | 285 | 1.19 | 0.045 3 | 0.004 1 | 0.136 3 | 0.012 5 | 0.021 5 | 0.000 5 | 484 | 169 | 130 | 11 | 137 | 3 |
| 25-17 | 4.1 | 114 | 150 | 0.76 | 0.054 8 | 0.006 6 | 0.147 1 | 0.018 5 | 0.020 4 | 0.000 7 | 406 | 272 | 139 | 16 | 130 | 4 |
| 25-18 | 4.2 | 154 | 145 | 1.07 | 0.056 1 | 0.004 0 | 0.147 6 | 0.009 2 | 0.020 1 | 0.000 8 | 454 | 159 | 140 | 8 | 128 | 5 |
| 25-20 | 5.4 | 189 | 190 | 1.00 | 0.053 8 | 0.005 3 | 0.139 6 | 0.013 7 | 0.019 2 | 0.000 6 | 361 | 226 | 133 | 12 | 122 | 3 |

**Table 3** U-Pb dating results for zircons from the granodiorite

| Sample Spot No. | Content (ppm) | | | Th/U | Isotopic ratios | | | | | | Isotopic age (Ma) | | | | | |
|---|---|---|---|---|---|---|---|---|---|---|---|---|---|---|---|---|
| | Pb | Th | U | | $^{207}Pb/^{206}Pb$ | ±1$\sigma$ | $^{207}Pb/^{235}U$ | ±1$\sigma$ | $^{206}Pb/^{238}U$ | ±1$\sigma$ | $^{207}Pb/^{206}Pb$ | ±1$\sigma$ | $^{207}Pb/^{235}U$ | ±1$\sigma$ | $^{206}Pb/^{238}U$ | ±1$\sigma$ |
| TKG-31 | | | | | | | | | | | | | | | | |
| 31-2 | 5.6 | 221 | 195 | 1.13 | 0.053 4 | 0.005 4 | 0.137 2 | 0.013 0 | 0.019 2 | 0.000 5 | 346 | 230 | 131 | 12 | 123 | 3 |
| 31-3 | 7.0 | 231 | 257 | 0.90 | 0.048 1 | 0.003 9 | 0.128 7 | 0.009 9 | 0.019 7 | 0.000 5 | 106 | 181 | 123 | 9 | 126 | 3 |
| 31-4 | 11.5 | 443 | 390 | 1.13 | 0.043 9 | 0.004 7 | 0.113 4 | 0.012 5 | 0.018 5 | 0.000 4 | 509 | 294 | 109 | 11 | 118 | 3 |
| 31-6 | 7.7 | 241 | 288 | 0.84 | 0.051 4 | 0.005 3 | 0.128 4 | 0.012 4 | 0.018 3 | 0.000 5 | 257 | 40 | 123 | 11 | 117 | 3 |
| 31-7 | 11.0 | 401 | 365 | 1.10 | 0.042 9 | 0.005 5 | 0.116 2 | 0.014 3 | 0.019 3 | 0.000 5 | 195 | 93 | 112 | 13 | 123 | 3 |
| 31-8 | 8.1 | 314 | 267 | 1.18 | 0.041 9 | 0.005 3 | 0.115 9 | 0.014 6 | 0.019 0 | 0.000 6 | 321 | 212 | 111 | 13 | 121 | 4 |
| 31-10 | 4.4 | 146 | 158 | 0.92 | 0.049 8 | 0.005 1 | 0.130 9 | 0.013 0 | 0.019 1 | 0.000 5 | 183 | 226 | 125 | 12 | 122 | 3 |
| 31-11 | 5.8 | 138 | 225 | 0.61 | 0.044 5 | 0.004 3 | 0.114 1 | 0.010 3 | 0.018 7 | 0.000 5 | 309 | 237 | 110 | 9 | 119 | 3 |
| 31-13 | 9.2 | 344 | 324 | 1.06 | 0.047 7 | 0.007 4 | 0.124 1 | 0.019 3 | 0.018 2 | 0.000 4 | 87 | 330 | 119 | 17 | 116 | 3 |
| 31-14 | 14.4 | 675 | 460 | 1.47 | 0.042 5 | 0.003 6 | 0.118 6 | 0.010 3 | 0.019 6 | 0.000 4 | 301 | 179 | 114 | 9 | 125 | 3 |
| 31-15 | 3.7 | 142 | 141 | 1.01 | 0.052 5 | 0.006 1 | 0.128 8 | 0.013 7 | 0.017 5 | 0.000 6 | 306 | 267 | 123 | 12 | 112 | 4 |
| 31-16 | 3.1 | 104 | 114 | 0.91 | 0.056 2 | 0.008 8 | 0.136 1 | 0.021 3 | 0.019 0 | 0.000 7 | 457 | 347 | 130 | 19 | 121 | 5 |
| 31-17 | 13.5 | 686 | 457 | 1.50 | 0.054 2 | 0.003 9 | 0.130 2 | 0.008 9 | 0.017 8 | 0.000 3 | 389 | 163 | 124 | 8 | 114 | 2 |
| 31-19 | 9.5 | 400 | 352 | 1.14 | 0.052 4 | 0.004 2 | 0.125 6 | 0.009 3 | 0.017 6 | 0.000 3 | 302 | 185 | 120 | 8 | 112 | 2 |
| 31-20 | 19.1 | 690 | 681 | 1.01 | 0.046 1 | 0.003 4 | 0.120 0 | 0.009 3 | 0.018 5 | 0.000 4 | 400 | 228 | 115 | 8 | 118 | 2 |

**Table 4** Sr and Nd isotopic compositions for the diorite and granodiorite in the Payangazu complex

| Sample | Petrology | Age (Ma) | Rb (ug/g) | Sr (ug/g) | $^{87}Rb/^{86}Sr$ | $^{87}Sr/^{86}Sr$ | ±2$\sigma$ | $(^{87}Sr/^{86}Sr)_i$ | Sm (ug/g) | Nd (ug/g) | $^{147}Sm/^{144}Nd$ | $^{143}Nd/^{144}Nd$ | ±2$\sigma$ | $(^{143}Nd/^{144}Nd)_t$ | $\varepsilon_{Nd}(t)$ | $T_{DM2}$ (Ma) |
|---|---|---|---|---|---|---|---|---|---|---|---|---|---|---|---|---|
| TKG-25 | Diorite | 130.5 | 82.6 | 309.2 | 0.772 | 0.709 999 | 0.000 003 | 0.708 6 | 4.57 | 24.43 | 0.112 7 | 0.512 318 | 0.000 003 | 0.512 22 | -4.8 | 1 319 |
| TKG-27 | Diorite | 130.5 | 100.0 | 279.0 | 1.036 | 0.711 961 | 0.000 004 | 0.710 0 | 4.73 | 25.30 | 0.112 6 | 0.512 316 | 0.000 004 | 0.512 22 | -4.9 | 1 323 |
| TKG-29 | Granodiorite | 118.4 | 166.9 | 300.3 | 1.606 | 0.714 454 | 0.000 004 | 0.711 8 | 5.89 | 29.25 | 0.121 2 | 0.512 133 | 0.000 004 | 0.512 04 | -8.7 | 1 623 |
| TKG-30 | Granodiorite | 118.4 | 171.3 | 291.1 | 1.702 | 0.714 611 | 0.000 003 | 0.711 7 | 5.47 | 30.10 | 0.109 4 | 0.512 122 | 0.000 004 | 0.512 04 | -8.8 | 1 627 |

The values used for calculation as follows: The decay constant of $^{147}Sm$ referred to Lugmair and Marti (1978); the current values of $(^{147}Sm/^{144}Nd)_{CHUR}$=0.196 7, $(^{143}Nd/^{144}Nd)_{CHUR}$=0.512 638 and $(^{147}Sm/^{144}Nd)_{DM}$=0.213 6 and $(^{143}Nd/^{144}Nd)_{DM}$=0.513 51 were applied; the current value of $(^{147}Sm/^{144}Nd)_{CC}$ referred to Jahn and Condie (1995)

series. The rocks are characterized by enriched LILE such Rb, Th, U and light REE and depleted HFSE including Nb, Ta, P, Ti and heavy REE, showing typical arc magmatic affinity (Ulmer, 2001; Kogiso et al., 1997; López-Escobar et al., 1993). The arc type affinity is obviously manifested by the diagrams of Rb vs. (Y+Nb) and Nb vs. Y (Pearce et al., 1984) (Fig. 7), as well as the Sr/Y vs. Y and La/Yb vs. Yb plots (Castillo et al., 1999; Defant and Drummond, 1993, Fig. 8). Furthermore, the abundant biotite and hornblende in the rocks imply high $H_2O$-contents of the magma, which is also consistent with features of hydrous arc magma (Ulmer, 2001).

The occurrence of granodiorite and quartz diorite with arc-type affinity suggests onset of an Early Cretaceous magmatism related to oceanic slab subduction, which is supported by chronological results of the sequence stratigraphy (Mitchell et al., 2012, 2007; Wang et al., 2012; Mitchell, 1993).

### 4.2.2 Magmatic source

The positive bulk rock $\varepsilon_{Hf}(t)$ value (0.6) and young $T_{DM}^{C}$ (1 147 Ma) of the quartz diorite, as well as the highly varied zircon $\varepsilon_{Hf}(t)$ values of -0.08 to -12.77 (Chen et al., 2016), indicate that the quartz diorite could not be derived directly from a

**Table 5** Whole-rock Hf isotopic compositions of the diorite and granodiorite

| Sample | Petrology | Age (Ma) | Lu | Hf | $^{176}Lu/^{177}Hf$ | $^{176}Hf/^{177}Hf$ | $2\sigma$ | $\varepsilon_{Hf}(t)$ | $T_{DM}^{C}$ (Ma) |
|---|---|---|---|---|---|---|---|---|---|
| TKG-25 | Diorite | 130.5 | 0.383 | 3.526 | 0.015 1 | 0.282 744 | 0.000 002 | 0.6 | 1 147 |
| TKG-31 | Granodiorite | 118.4 | 0.421 | 4.996 | 0.011 7 | 0.282 522 | 0.000 002 | -7.2 | 1 627 |
| TKG-32 | Granodiorite | 118.4 | 0.406 | 5.661 | 0.010 0 | 0.282 576 | 0.000 002 | -5.1 | 1 498 |

The values used for calculation as follows: The decay constant of $^{176}Lu$ referred to Scherer et al. (2001); the current values of $(^{176}Lu/^{177}Hf)_{CHUR}$=0.033 2, $(^{176}Hf/^{177}Hf)_{CHUR}$=0.282 772 and $(^{176}Lu/^{177}Hf)_{DM}$=0.038 4, $(^{176}Hf/^{177}Hf)_{DM}$= 0.283 25 referred to Blichert-Toft et al. (1997); the current values of $(^{176}Lu/^{177}Hf)_{CC}$=0.015 0 referred to Goodge and Vervoort (2006).

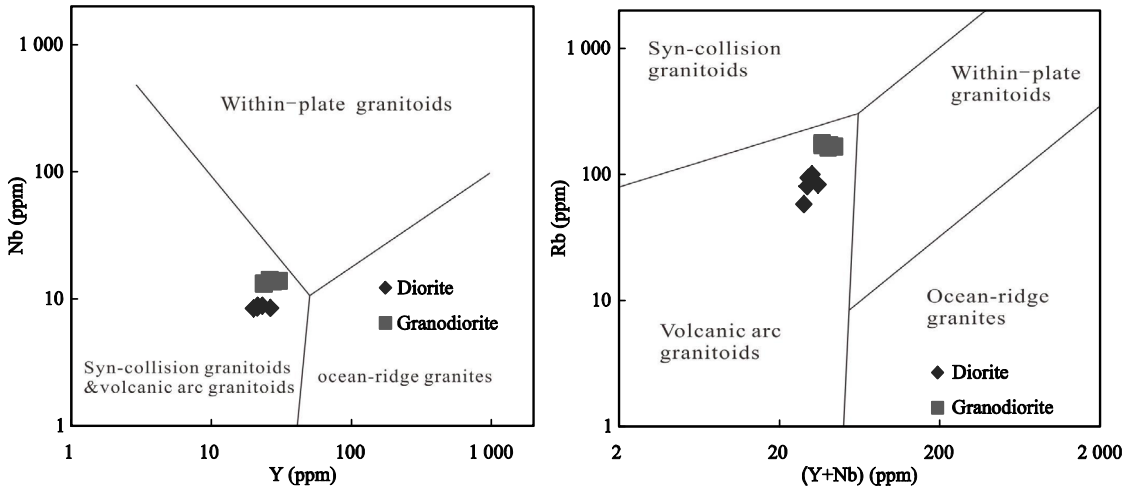


**Figure 7.** Rb vs. (Y+Nb) and Nb vs. Y discrimination diagrams (Pearce et al., 1984).

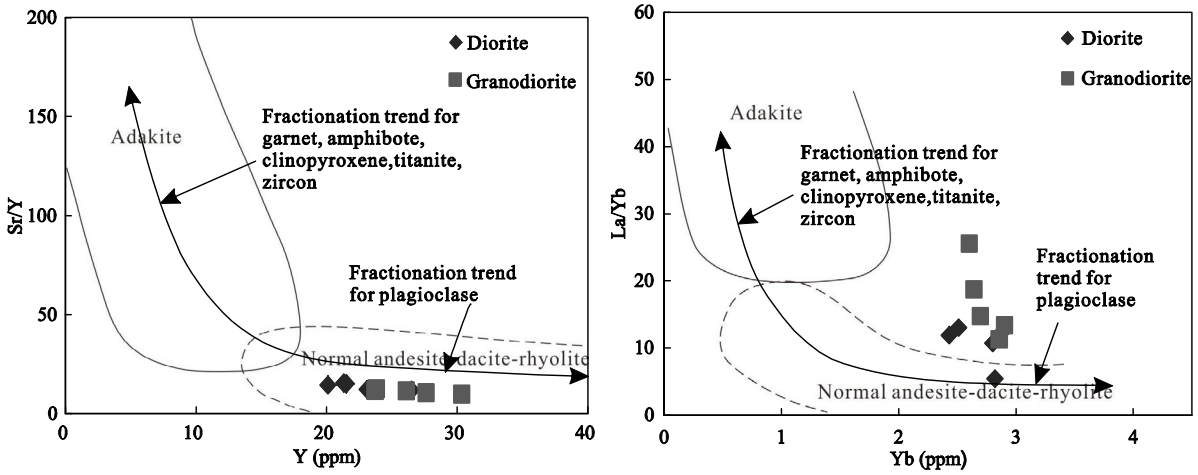


**Figure 8.** Discrimination diagrams for adakite and island-arc andesite-dacite-rhyolite. (a) Sr/Y vs. Y (Defant and Drummond, 1993); (b) La/Yb vs. Yb (Castillo et al., 1999). Fractionation trend of minerals are after Richards and Kerrich (2007).

mantle or crust source alone (Fig. 9). On the contrary, a mixed source of mantle and crustal materials can be inferred. Indeed, the negative $\varepsilon_{Nd}(t)$ (-4.8 and -4.9) and relatively high $(^{87}Sr/^{86}Sr)_i$ (0.708 6 and 0.710 0) of the quartz diorite are projected near the bivariate hybrid line (Fig. 10) of the Early Cretaceous Tethyan basalt and lower crust with a lower crustal contribution of about 60%. Therefore, the quartz diorite was likely derived from a mixed source of the mantle and the lower crustal components. In comparison, the granodiorite has bulk rock $\varepsilon_{Hf}(t)$ values (-7.2 and -5.1) lower than that of the quartz diorite, which may reflect higher crustal contribution in the magma source. And consistently, the granodiorite samples are projected near the mixing line on the $\varepsilon_{Nd}(t)$ vs. initial Sr isotope ratio diagram (Fig. 10) and suggest that the lower crustal contribution is around 85%.

The $Mg^{\#}$ is an effective indicator in discriminating the mantle or crust source of magmas. Experimental petrological results have shown that melts from the lower crust have $Mg^{\#}$ below 40 regardless of the degree of partial melting, whereas melts with $Mg^{\#}$ higher than 40 require a contribution of mantle component (Rapp and Watson, 1995). Here, the $Mg^{\#}$ values (Table 1) of the quartz diorite and granodiorite are 46.9–50.2 and 41.4–42.8 respective, both of which are higher than 40, suggestive of the mantle contribution. In addition, the contemporaneous mafic dikes (Chen et al., 2016) in the complex also support the involvement of mantle materials in magmas. Thus,

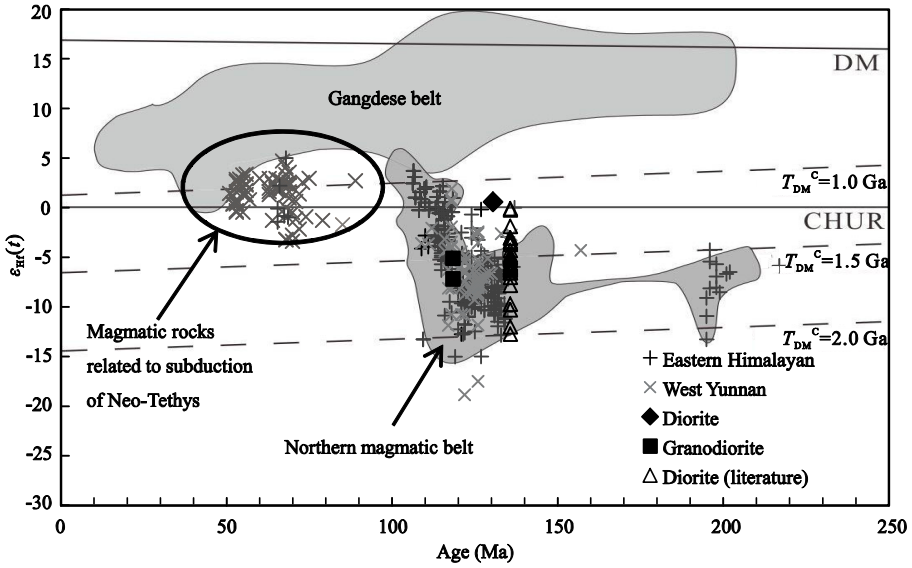


**Figure 9.** $\varepsilon_{Hf}(t)$ vs. age diagram of granitoids in the central Myanmar and other areas of the Tethyan tectonic region. Data sources: Gangdese batholiths (Zhu et al., 2011, 2009a; Ji et al., 2009; Chu et al., 2006); Northern magmatic belt (Zhu et al., 2011, 2009a; Chu et al., 2006); Eastern Himalayan (Chiu et al., 2009; Zhu et al., 2009b; Liang et al., 2008); West Yunnan (Xu et al., 2012; Liang et al., 2008); Diorite (literature) (Chen et al., 2016). The lines of crustal extraction are calculated by current value of $(^{176}Lu/^{177}Hf)_{CC}$=0.015 0 from average continental crust (Goodge and Vervoort, 2006).

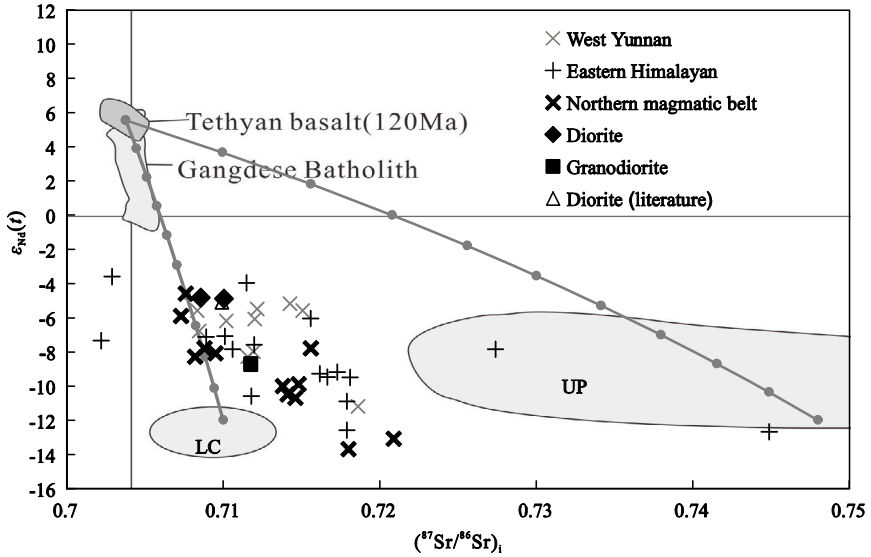


**Figure 10.** $\varepsilon_{Nd}(t)$ vs. $(^{87}Sr/^{86}Sr)_i$ diagrams of the Early Cretaceous granitoids in the central Myanmar and the other areas of the Tethyan tectonic system. Data sources: Gangdese batholiths (Wen et al., 2008); Northern magmatic belt (Zhu et al., 2009a); Eastern Himalayan (Lin et al., 2012; Zhu et al., 2009b); West Yunnan (Yang et al., 2006). UC. Upper crust; LC. lower crust.

the genesis of the quartz diorite and granodiorite is related to a mixed source of the mantle and crustal component.

#### 4.2.3 Petrogenesis of the complex

As discussed above, the trace element concentrations of the quartz diorite and granodiorite show arc-type magmatic affinity while their Sr-Nd-Hf isotopes demonstrate a magma source of a mixture of mantle and crustal components; therefore, the complex was most likely formed in a subduction setting. In subduction setting, the generation of magmas is related to interactions among the subducted oceanic crust, the overlying mantle wedge and the crust. Partial melting of basaltic slab with plagioclase completely consumed would produce adakitic magmas (Martin et al., 2005; Peacock et al., 1994; Mcdonough, 1991; Defant and Drummond, 1990). The lower Sr contents (Table 1, Fig. 8) of the quartz diorite and granodiorite of this study suggest that melting of subducted slab was insignificant if any. Nevertheless, dehydration of subducted slab is necessary to metasomatize the overlying mantle wedge, a key process to generate arc magmas (Ulmer, 2001; López-Escobar et al., 1993). Thus, it seems that the fluid released by dehydration of slab with or without melting (maybe include melting of the subducted sediments) and its subsequent interaction with the overlying mantle wedge triggered the partial melting of the mantle and generated the initial arc magmas. However, the initial magmas generated in mantle wedge were generally basaltic (Hattori and Guillot, 2003; Schmidt and Poli, 1998; Peacock, 1993). The addition of the lower crustal component was most likely a scenario that underplating of the initially mantle-derived magmas at the base of the lower crust led to the partial melting of lower crust which formed the crustal melts that subsequently mixed with the mantle magmas (Wörner et al., 1992; Hildreth and Moorbath, 1988).

In addition to the higher contribution of the lower crust, deviations of the quartz diorite and granodiorite from the bivariate hybrid line may result from assimilation of mid-upper crust during the ascent and emplacement of the mixed magmas (Fig. 10). Besides, the granodiorite has decreasing $Al_2O_3$, CaO, $Fe_2O_3{}^T$, MgO, $Na_2O$ contents and obviously increasing $K_2O$ content (Fig. 11), higher large-ion lithophile elements (LILE) (Fig. 4) in comparison with quartz diorite. This maybe resulted from various degrees of contribution of lower crust and/or assimilation of mid-upper crust. Thus, assimilation may play a role in magmatic evolution. On the other hand, the weakly negative Eu anomalies and low Sr contents of the quartz diorite and granodiorite may result from fractionation of plagioclase (Figs. 4 and 8, Table 2). However, the smooth MREE (middle REE) and HREE patterns (Fig. 4), and high Y and Yb contents (Fig. 8, Table 2) show little fractionation of garnet and hornblende. In summary, the possible scenario of magma origination and evolution for the Payangazu complex might be that ascent of mantle magmas at the base of the lower crust resulted in partial melting of the lower crust, where the resultant melts subsequently mixed with the mantle magmas; and during subsequent ascent and emplacement, the magmas experienced assimilation of mid-upper crust and fractionation of plagioclase. The near 10 Ma temporal interval between the quartz diorite and granodiorite may indicate a prolonged interaction between mantle-derived magma and lower crust or the mixed melt and the mid-upper crust which was responsible for the more silicic granodiorite with lower $\varepsilon_{Hf}(t)$ and $\varepsilon_{Nd}(t)$ values.

### 4.3 Tectonic Implications

The Tethyan tectonic domain in China could be divided as the Gangdese belt, the northern magmatic belt, the eastern Himalayan, and the western Yunnan (Fig. 12). The Gangdese belt is composed of the Early Jurassic to Paleogene intrusions with positive $\varepsilon_{Hf}(t)$, $\varepsilon_{Nd}(t)$, and low $(^{87}Sr/^{86}Sr)_i$ values, and was thought to be generated by subduction and subsequent roll-back of Neo-Tethyan slab (Ma et al., 2017; Zhu et al., 2011, 2009a; Ji et al., 2009; Wen et al., 2008; Chu et al., 2006; Figs. 9, 10).

Intrusions with I-type affinities are widespread in the northern magmatic belt, the eastern Himalaya, and western Yunnan; however, those in the northern magmatic belt mainly emplaced in the Early Cretaceous (Zhu et al., 2011, 2009a; Chu et al., 2006; Fig. 9), whereas those in the eastern Himalaya and western Yunnan were formed in the Early Cretaceous and Late Cretaceous to Paleogene (Lin et al.; 2012; Xu et al., 2012; Chiu et al., 2009; Zhu et al., 2009b; Liang et al., 2008; Yang et al., 2006; Fig. 9). Formation of the I-type intrusions in the East Himalaya and the West Yunnan was suggested to have been formed under post-collisional setting subsequent to the closure of the Bagong-Nujiang Ocean (part of the Mesotethyan Ocean) in Late Jurassic–Early Cretaceous (Xu et al., 2012; Chiu et al., 2009). However, the occurrences of the contemporaneous volcanic rocks with obvious arc-type signatures in eastern Himalaya argue against a post-collisional region (Lin et al., 2012). A link between the Early Cretaceous I-type intrusions and volcanic rocks in the eastern Himalaya and subduction of Neo-Tethys was proposed by Lin et al. (2012). However, the ages of emplacement for these intrusions are significantly older than the Neo-Tethyan subduction related intrusions in Myanmar (the Wuntho-Popa arc), the Gangdese, the East Himalaya, and the West Yunnan (Wang et al., 2014; Mitchell et al., 2012; Xu et al., 2012; Chiu et al., 2009; Ji et al., 2009). In addition, Sr-Nd-Hf isotope compositions of these intrusions are distinct from those related to the Neo-Tethyan subduction which are characterized by positive $\varepsilon_{Hf}(t)$ and low $(^{87}Sr/^{86}Sr)_i$, high $\varepsilon_{Nd}(t)$ values (Wang et al., 2014; Mitchell et al., 2012, Xu et al., 2012; Chiu et al., 2009; Ji et al., 2009; Figs. 9, 10). Therefore, the Early Cretaceous intrusions in central Myanmar, eastern Himalaya and western Yunnan have nothing to do with the subduction of Neo-Tethyan Ocean.

The relationship between the Early Cretaceous I-type magmatism and the subduction of the Bangong-Nujiang Ocean is also supported by previous works, for instance, the Early Cretaceous I-type intrusions in the northern belts, the eastern Himalaya, and the western Yunnan were speculated to be related to the subduction of the Bangong-Nujiang oceanic slab (Zhu et al., 2009a, b; Yang et al., 2006). The association of the Early Cretaceous I-type magmatism with the Bangong-Nujiang oceanic slab subduction can well explain their arc-type affinities and distribution as well, i.e., these Early Cretaceous intrusions occur closer to the Bangong-Nujiang suture in the eastern Himalaya and the western Yunnan (Xu et al., 2012; Chiu et al., 2009) rather thant the suture of the Neo-Tethyan Ocean.

The quartz diorite and granodiorite of the Payangazu complex in the central Myanmar belong to the Mogok-Mandalay-Mergui belt and have geochemical features of subduction related arc magmatism, and show geochemical characteristics similar to the Early Cretaceous counterparts in the north magmatic belt, the eastern Himalaya and the western Yunnan, and thus they were likely formed in similar tectonic setting. Considering the fact that these Early Cretaceous intrusions have Sr-Nd-Hf isotopic features similar to the contemporaneous I-type intrusions in the northern magmatic belt, eastern Himalaya and western Yunnan (Xu et al., 2012; Zhu et al., 2011, 2009a, b; Liang et al., 2008; Yang et al., 2006; Figs. 9, 10), formation of these Early Cretaceous intrusions is most likely related to the Bangong-Nujiang Ocean (part of the Tethyan System). Therefore, the Bangong-Nujiang Ocean might extend into the central Myanmar through the eastern Himalaya Syntaxis. In fact, the south extension of the Bangong-Nujiang Ocean to the western Yunnan and Myanmar was proposed by some researchers (Mitchell et al., 2012; Wang et al., 2012; Mo et al., 1994), while this study further demonstrated that the Bangong-Nujiang Ocean might extend far south to the central Myanmar.

## 5 CONCLUSIONS

(1) The quartz diorite and granodiorite in the Payangazu complex, have zircon ages of 130.5±4.0 (MSWD=3.5) and 118.4±2.5 Ma (MSWD=2.4), respectively.

(2) Both the quartz diorite and granodiorite are metaluminous, enriched in LILE like LREE, Rb, Th, and U, and depleted in HFSE such as HREE, Nb, Ta, P, and Ti, indicative of arc-type magmatic affinities.

(3) The isotopic data together with the high $Mg^{\#}$ of the quartz diorite and granodiorite suggest a strong involvement of mantle materials in the genesis of the parent magmas. The possible petrogenetic process may be that ascent of mantle melts from the metasomatized mantle wedge at the base of the lower crust resulted in partial melting of the lower crust, where

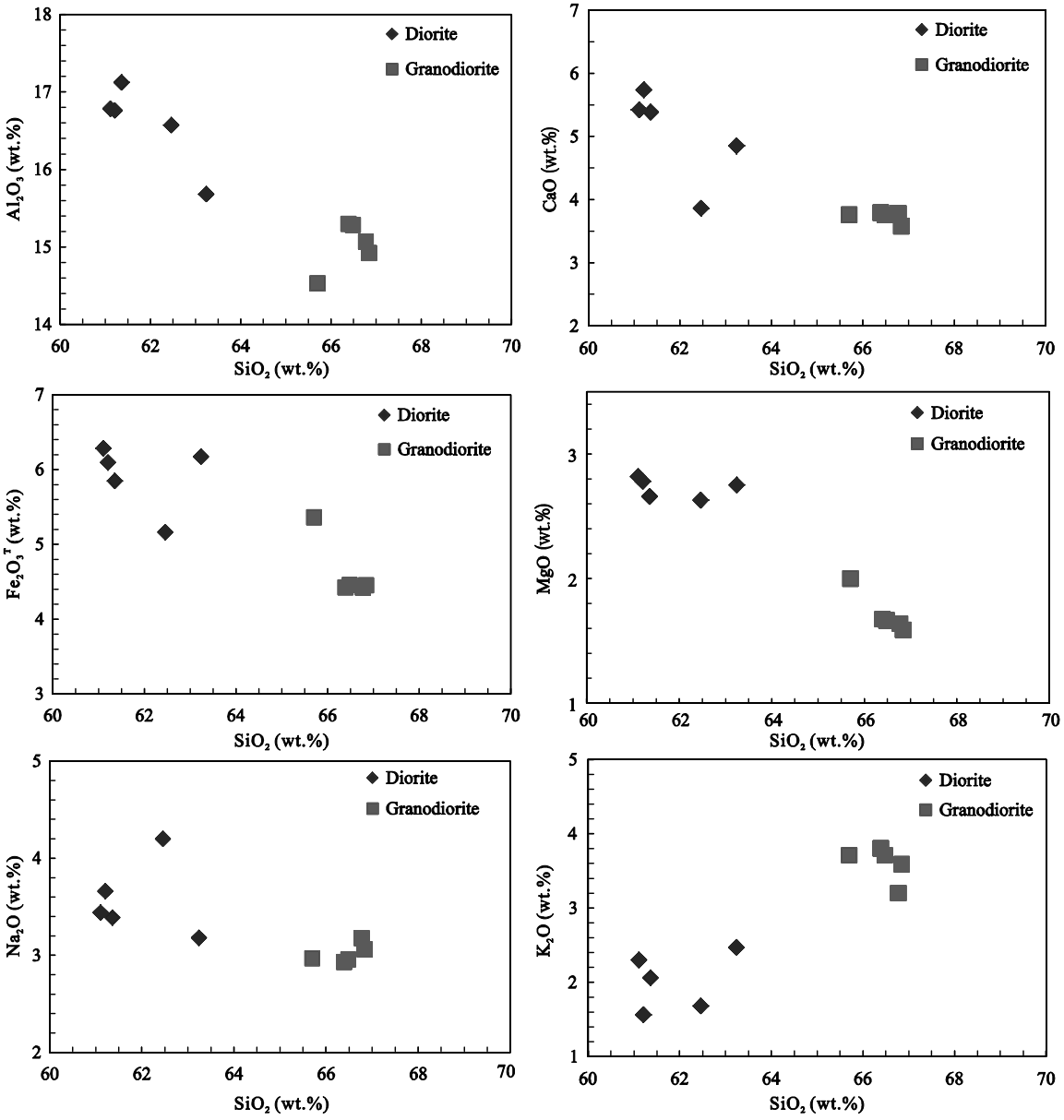


**Figure 11.** Variations of major elements vs. $SiO_2$ content (wt.%).

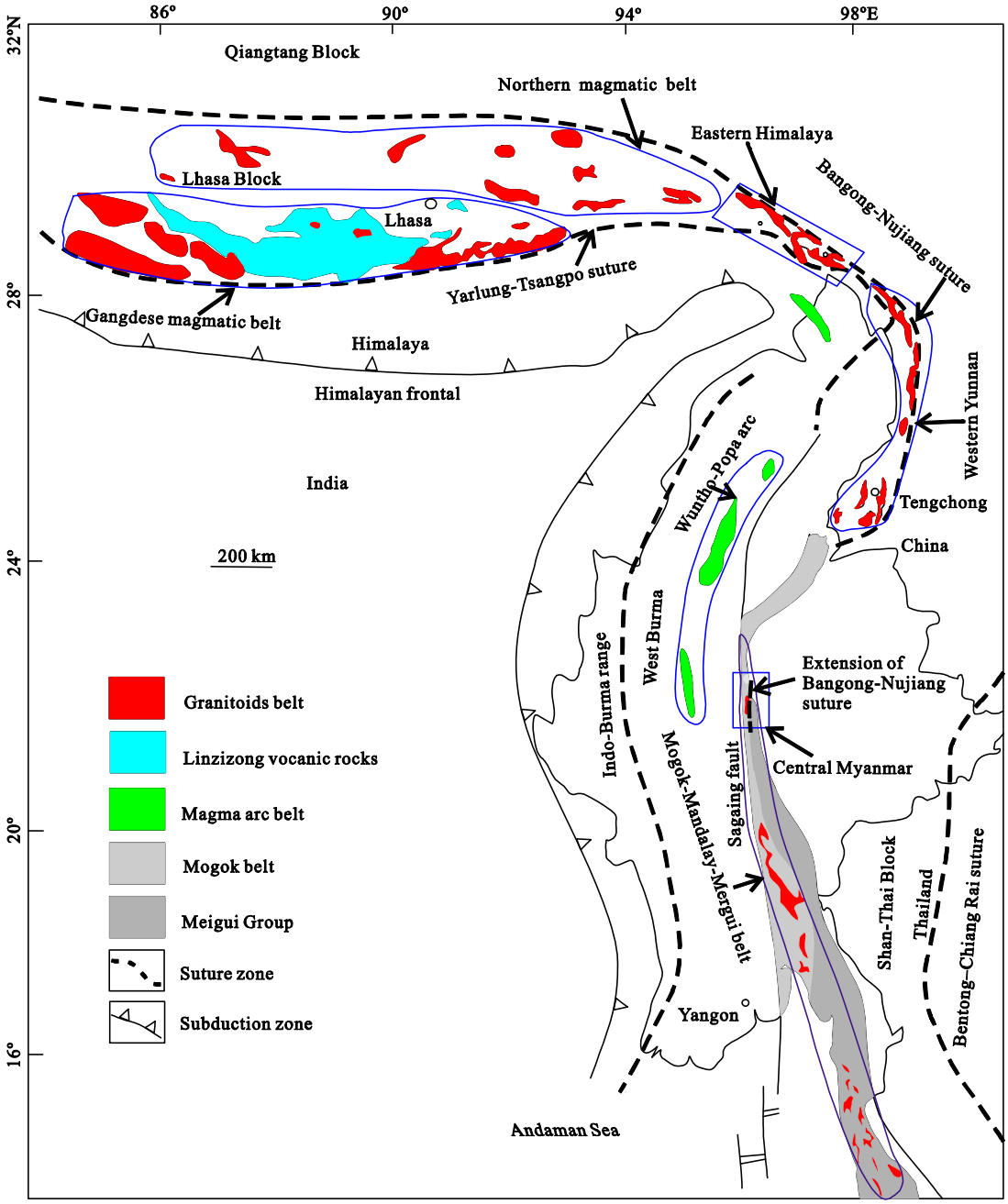


**Figure 12.** Simplified tectonic framework of Tethys showing the south extension of the Bangong-Nujiang suture (modified from Xu et al. 2012).

the resultant melts subsequently mixed with the mantle magmas, and late stage assimilation of mid-upper crust and fractionation of plagioclase may be also involved during their subsequent ascent and emplacement.

(4) The Early Cretaceous intrusions in the central Myanmar were most likely related to the southward subduction of the Bangong-Nujiang Ocean and the Bangong-Nujiang Ocean might extend far south to the central Myanmar.

## ACKNOWLEDGMENTS

This Study was supported by the National Key R & D Program of China (No. 2016YFC0600407) and the Natural Science Foundation of China (Nos. 41772065, 41421062). We thank Dr. Swe Win, Mr. Kyaing Sein and Soe Thura Tun for their assistance during our fieldwork. The final publication is available at Springer via https://doi.org/10.1007/s12583-018-0862-9.

## REFERENCES CITED

Barber, A. J., Crow, M. J., Milsom, J. S, 2005. Sumatra: Geology, Resources and Tectonic Evolution. *Geological Society Memoirs*, *London*, 31: 1–248

Barley, M. E., Pickard, A. L., Zaw, K. et al., 2003. Jurassic to Miocene Magmatism and Metamorphism in the Mogok Metamorphic Belt and the India-Eurasia Collision in Myanmar. *Tectonics*, 22(3): 4–14. https://doi.org/10.1029/2002TC001398

Bertrand, G., Rangin, C., Maluski, H., 2001. Diachronous Cooling along the

Mogok Metamorphic Belt (Shan Scarp, Myanmar): The Trace of the Northward Migration of the Indian Syntaxis. *Journal of Asian Earth Sciences*, 19(5): 649–659. https://doi.org/10.1016/S1367-9120(00)00061-4

Black, L. P., Kamo, S. L., Allen, C. M., et al., 2003. Temora 1: A New Zircon Standard for Phanerozoic U-Pb Geochronology. *Chemical Geology*, 200(1/2): 155–170. https://doi.org/10.1016/S0009-2541(03)00165-7

Blichert-Toft, J., Gleason, J. D., Télouk, P. et al., 1997. The Lu-Hf Isotope Geochemistry of Shergottites and the Evolution of the Martian Mantle-Crust System. *Earth and Planetary Science Letters*, 154(1/2/3/4): 243–258. https://doi.org/10.1016/S0012-821X(99)00222-8

Castillo, P. R., Janney, P. E., Solidum, R. U., 1999. Petrology and Geochemistry of Camiguin Island, Southern Philippines: Insights to the Source of Adakites and Other Lavas in a Complex Arc Setting. *Contributions to Mineralogy & Petrology*, 134(1): 33–51. https://doi.org/10.1007/s004100050467

Chen, X. J., Xu, Z. Q., Sein, K., et al., 2016. The Early Cretaceous Tectonic Magmatism in the Mogok District, Central Myanmar, and Its Implication for the Evolution of Tethy. *Acta Geologica Sinica*, 90(11): 3060–3080. https://doi.org/10.3969/j.issn.0001-5717.2016.11.007 (in Chinese with English Abstract)

Chiu, H. Y., Chung, S. L., Wu, F. Y., et al., 2009. Zircon U-Pb and Hf Isotopic Constraints from Eastern Transhimalayan Batholiths on the Precollisional Magmatic and Tectonic Evolution in Southern Tibet. *Tectonophysics*, 477(1/2): 3–19. https://doi.org/10.1016/j.tecto.2009.02.034

Chu, M. F., Chung, S. L., Song, B., et al., 2006. Zircon U-Pb and Hf Isotope Constraints on the Mesozoic Tectonics and Crustal Evolution of Southern Tibet. *Geology*, 34(9): 745–752. https://doi.org/10.1130/G22725.1

Curray, J. R., 2005. Tectonics and History of the Andaman Sea Region. *Journal of Asian Earth Sciences*, 25(1): 187–232. https://doi.org/10.1016/j.jseaes.2004.09.001

Defant, M. J., Drummond, M. S., 1990. Derivation of Some Modern Arc Magmas by Melting of Young Subducted Lithosphere. *Nature*, 347(6294): 662–665. https://doi.org/10.1038/347662a0

Defant, M. J., Drummond, M. S., 1993. Mount St. Helens: Potential Example of the Partial Melting of the Subducted Lithosphere in a Volcanic Arc. *Geology*, 21(6): 547–550. https://doi.org/10.1130/0091-7613(1993)021%3C0547:MSHPEO%3E2.3.CO;2

Gardiner, N. J., Searle, M. P., Robb, L. J., 2015. Neo-Tethyan Magmatism and Metallogeny in Myanmar—An Andean Analogue? *Journal of Asian Earth Sciences*, 106(1): 197-215. https://doi.org/10.1016/j.jseaes.2015.03.015

Goffé, B., Rangin, C., Maluski, H., 2002. Jade and Associated Rocks from the Jade Mines Area, Northern Myanmar as Record of a Polyphased High-pressure Metamorphism. Asian Earth Sci., 20: 16–17

Goodge, J. W., Vervoort, J. D., 2006. Origin of Mesoproterozoic A-Type Granites in Laurentia: Hf Isotope Evidence. *Earth and Planetary Science Letters*, 243(3): 711–731. https://doi.org/10.1016/j.epsl.2006.01.040

Goto, A. Tatsumi, Y., 1996. Quantitative Analysis of Rock Samples by an X-Ray Fluorescence Spectrometer (II). *The Rigaku Journal*, 13(2): 20–38

Hattori, K. H., Guillot, S., 2003. Volcanic Fronts Form as a Consequence of Serpentinite Dehydration in the Forearc Mantle Wedge. *Geology*, 31(6): 525–528. https://doi.org/10.1130/0091-7613(2003)031<0525:VFFAAC>2.0.CO;2

Hildreth, W., Moorbath, S., 1988. Crustal Contributions to Arc Magmatism in the Andes of Central Chile. *Contributions to Mineralogy and Petrology*, 98(4): 455–489. https://doi.org/10.1007/BF00372365

Hoskin, P. W. O., 2003. The Composition of Zircon and Igneous and Metamorphic Petrogenesis. *Reviews in Mineralogy and Geochemistry*, 53(1): 27–62. https://doi.org/10.2113/0530027

Huangfu, P. P., Wang, Y., Li, Z., et al., 2016. Effects of Crustal Eclogitization on Plate Subduction-Collision Dynamics: Implications for India-Asia Collision. *Journal of Earth Science*, 27(5): 727–739. https://doi.org/10.1007/s12583-016-0701-9

Jahn, B. M., Condie, K. C., 1995. Evolution of the Kaapvaal Craton as Viewed from Geochemical and Sm-Nd Isotopic Analyses of Intracratonic Pelites. *Geochimica et Cosmochimica Acta*, 59(11): 2239–2258. https://doi.org/10.1016/0016-7037(95)00103-7

Ji, W. Q., Wu, F. Y., Chung, S. L., et al., 2009. Zircon U-Pb Geochronology and Hf Isotopic Constraints on Petrogenesis of the Gangdese Batholith, Southern Tibet. *Chemical Geology*, 262(3/4): 229–245. https://doi.org/10.1016/j.chemgeo.2009.01.020

Jiang, H., Li, W. Q., Jiang, S. Y., et al., 2017. Geochronological, Geochemical and Sr-Nd-Hf Isotopic Constraints on the Petrogenesis of Late Cretaceous A-type Granites from the Sibumasu Block, Southern Myanmar, SE Asia. *Lithos*, 268–271: 32–47. https://doi.org/10.1016/j.lithos.2016.11.005

Kogiso, T., Tatsumi, Y., Nakano, S., 1997. Trace Element Transport during Dehydration Processes in the Subducted Oceanic Crust: 1. Experiments and Implications for the Origin of Ocean Island Basalts. *Earth and Planetary Science Letters*, 148(1/2): 193–205. https://doi.org/10.1016/S0012-821X(97)00018-6

Li, X. H., Li, Z. X., Wingate, M. T. D., et al., 2006. Geochemistry of the 755 Ma Mundine Well Dyke Swarm, Northwestern Australia: Part of a Neoproterozoic Mantle Superplume Beneath Rodinia?. *Precambrian Research*, 146(1/2): 1–15. https://doi.org/10.1016/j.precamres.2005.12.007

Liang, Y., S., Chung, D., Liu, Y., et al., 2008. Detrital Zircon Evidence from Burma for Reorganization of the Eastern Himalayan River System. *American Journal of Science*, 308(4): 618–638. https://doi.org/10.2475/04.2008.08

Lin, I. J., Chung, S. L., Chu, C. H., et al., 2012. Geochemical and Sr-Nd Isotopic Characteristics of Cretaceous to Paleocene Granitoids and Volcanic rocks, SE Tibet: Petrogenesis and Tectonic Implications. *Journal of Asian Earth Sciences*, 53(7): 131–150. https://doi.org/10.1016/j.jseaes.2012.03.010

Liu, Y., Hu, Z., Gao, S., et al., 2008. *In situ* Analysis of Major and Trace Elements of Anhydrous Minerals by LA-ICP-MS without Applying an Internal Standard. *Chemical Geology*, 257(1-2): 34–43. https://doi.org/10.1016/j.chemgeo.2008.08.004

Liu, Y., Liu, H. C., Li X. H., 1996. Simultaneous and Precise Determination of 40 Trace Elements in Rock Samples Using ICP-MS. *Geochimica*, 25(6): 552–558 (in Chinese with English Abstract)

López-Escobar, L., Killian, R., Kempton, P., et al., 1993. Petrography and Geochemistry of Quaternary Rocks from the Southern Volcanic Zone between 41°30' and 46°00'S, Chile. *Andean Geology*, 20(1): 33–55. https://doi.org/10.5027/andgeoV20n1-a04

Ludwig, K. R., 2003. Isoplot/Ex Version 3.00: A Geochronological Toolkit for Microsoft Excel. Geochronology Center Special Publication, Berkeley. 4: 37

Lugmair, G. W., Marti, K., 1978. Lunar Initial $^{143}Nd/^{144}Nd$: Differential

Evolution of the Lunar Crust and Mantle. *Earth and Planetary Science Letters*, 39(3): 349–357. https://doi.org/10.1016/0012-821X(78)90021-3

Ma, X., Xu, Z., Chen, X., et al., 2017. The Origin and Tectonic Significance of the Volcanic Rocks of the Yeba Formation in the Gangdese Magmatic Belt, South Tibet. *Journal of Earth Science*, 28(2): 265–282. https://doi.org/10.1007/s12583-016-0925-8

Maniar, P. D., Piccoli, P. M., 1989. Tectonic Discrimination of Granitoids. *Geological Society of America Bulletin*, 101(5): 635–643. https://doi.org/10.1130/0016-7606(1989)101<0635:TDOG>2.3.CO;2

Martin, H., Smithies, R. H., Rapp, R., et al., 2005. An Overview of Adakite, Tonalite-Trondhjemite-Granodiorite (TTG), and Sanukitoid: Relationships and Some Implications for Crustal Evolution. *Lithos*, 79(1/2): 1–24. https://doi.org/10.1016/j.lithos.2004.04.048

Maurin, T., Masson, F., Rangin, C., et al., 2010. First Global Positioning System Results in Northern Myanmar: Constant and Localized Slip Rate along the Sagaing Fault. *Geology*, 38(7): 591–594. https://doi.org/10.1130/G30872.1

Mcdonough, W. F., 1991. Partial Melting of Subducted Oceanic Crust and Isolation of Its Residual Eclogitic Lithology. *Philosophical Transactions of the Royal Soceity*, 335(1638): 407–418. https://doi.org/10.1098/rsta.1991.0055

Metcalfe, I., 1988. Origin and Assembly of South-East Asian Continental Terranes. *Geological Society*, *London*, *Special Publications*, 37: 101–118. https://doi.org/10.1144/GSL.SP.1988.037.01.08

Metcalfe, I., 2013. Gondwana Dispersion and Asian Accretion: Tectonic and Palaeogeographic Evolution of Eastern Tethys. *Journal of Asian Earth Sciences*, 66: 1–33. https://doi.org/10.1016/j.jseaes.2012.12.020

Middlemost, E. A., 1994. Naming Materials in the Magma/Igneous Rock System. *Earth-Science Reviews*, 37(3/4): 215–224. https://doi.org/10.1016/0012-8252(94)90029-9

Mitchell, A. H. G., 1977. Tectonic Settings for Emplacement of Southeast Asian Tin Granites. *Bulletin of the Geological Society of Malaysia*, 9: 123–140

Mitchell, A. H. G., 1992. Late Permian–Mesozoic Events and the Mergui Group Nappe in Myanmar and Thailand. *Journal of Southeast Asian Earth Sciences*, 7(2/3): 165–178. https://doi.org/10.1016/0743-9547(92)90051-C

Mitchell, A. H. G., Htay, M. T., Htun, K. M., et al., 2007. Rock Relationships in the Mogok Metamorphic Belt, Tatkon to Mandalay, Central Myanmar. *Journal of Asian Earth Sciences*, 29(5): 891–910. https://doi.org/10.1016/j.jseaes.2006.05.009

Mitchell, A., 1993. Cretaceous–Cenozoic Tectonic Events in the Western Myanmar (Burma)-Assam Region. *Journal of the Geological Society*, 150(6): 1089–1102. https://doi.org/10.1144/gsjgs.150.6.1089

Mitchell, A., Chung, S. L., Oo, T., et al., 2012. Zircon U-Pb Ages in Myanmar: Magmatic-Metamorphic Events and the Closure of a Neo-Tethys Ocean?. *Journal of Asian Earth Sciences*, 56(3): 1–23. https://doi.org/10.1016/j.jseaes.2012.04.019

Mo, X. X., Deng, J., Lu, F., 1994. Volcanism and the Evolution of Tethys in Sanjiang Area, Southwestern China. *Journal of Southeast Asian Earth Sciences*, 9(4): 325–333. https://doi.org/10.1016/0743-9547(94)90043-4

Peacock, S. M., 1993. Large-Scale Hydration of the Lithosphere above Subducting Slabs. *Chemical Geology*, 108(12/3/4): 49–59. https://doi.org/10.1016/0009-2541(93)90317-C

Peacock, S. M., Rushmer, T., Thompson, A. B., 1994. Partial Melting of Subducting Oceanic Crust. *Earth and Planetary Science Letters*, 121(1/2): 227–244. https://doi.org/10.1016/0012-821X(94)90042-6

Pearce, J. A., Harris, N. B. W., Tindle, A. G., 1984. Trace Element Discrimination Diagrams for the Tectonic Interpretation of Granitic Rocks. *Journal of Petrology*, 25(4): 956–983. https://doi.org/10.1093/petrology/25.4.956

Peccerillo, A., Taylor, S. R., 1976. Geochemistry of Eocene Calc-Alkaline Volcanic Rocks from the Kastamonu Area, Northern Turkey. *Contributions to Mineralogy and Petrology*, 58(1): 63–81. https://doi.org/10.1007/BF00384745

Prosanta, K. K., Shamim, S., Manoranjan, M., et al., 2017. Myanmar-Andaman-Sumatra Subduction Margin Revisited: Insights of Arc-Specific Deformations. *Journal of Earth Science*, 28(4): 1–12. https://doi.org/10.1007/s12583-017-0752-6

Rapp, R. P., Watson, E. B., 1995. Dehydration Melting of Metabasalt at 8–32 kbar: Implications for Continental Growth and Crust-Mantle Recycling. *Journal of Petrology*, 36(4): 891–931. https://doi.org/10.1093/petrology/36.4.891

Richards, J. P., Kerrich, R., 2007. Special Paper: Adakite-Like Rocks: Their Diverse Origins and Questionable Role in Metallogenesis. *Economic Geology*, 102(4): 537–576. https://doi.org/10.2113/gsecongeo.102.4.537

Rollinson, H., 1993. Using Geochemical Data: Evaluation, Presentation, Interpretation. Longman Group, London. 1–352

Scherer, E., Münker, C., Mezger, K., 2001. Calibration of the Lutetium-Hafnium Clock. *Science*, 293: 683–687. https://doi.org/10.1126/science.1061372

Schmidt, M. W., Poli, S., 1998. Experimentally Based Water Budgets for Dehydrating Slabs and Consequences for Arc Magma Generation. *Earth and Planetary Science Letters*, 163: 361–379. https://doi.org/10.1016/S0012-821X(98)00142-3

Searle, M. P., Noble, S. R., Cottle, J. M., et al., 2007. Tectonic Evolution of the Mogok Metamorphic Belt, Burma (Myanmar) Constrained by U-Th-Pb Dating of Metamorphic and Magmatic Rocks. *Tectonics*, 26(3): 623–626. https://doi.org/10.1029/2006TC002083

Sun, S. S., McDonough, W. F., 1989. Chemical and Isotopic Systematics of Oceanic Basalts: Implications for Mantle Composition and Processes. *Geological Society*, *London*, *Special Publications*, 42(1): 313–345. https://doi.org/10.1144/GSL.SP.1989.042.01.19

Tu, X. L., Hong Z., Deng, W. F., et al., 2011. Application of Resolution *in-situ* Laser Ablation ICP-MS in Trace Element Analyses. *Geochimica*, 40(1): 308–313. https://doi.org/10.19700/j.0379-1726.2011.01.009 (in Chinese with English Abstract)

Ulmer, P., 2001. Partial Melting in the Mantle Wedge—The Role of $H_2O$ in the Genesis of Mantle-Derived 'Arc-Related' Magmas. *Physics of the Earth and Planetary Interiors*, 127(1/2/3/4): 215–32. https://doi.org/10.1016/S0031-9201(01)00229-1

Waltham, T., 2010. The Ruby Mines of Mogok. *Geology Today*, 15(4): 143–149. https://doi.org/10.1046/j.1365-2451.1999.1504007.x

Wang, H., Lin, F. C., Li, X. Z., et al., 2012, Tectonic Unit Division and Neo-Tethys Tectonic Evolution in North-Central Myanmar and Its Adjacent Areas. *Geology in China*, 39(4): 912–922 (in Chinese with English Abstract)

Wang, J. G., Wu, F. Y., Tan, X. C., et al., 2014. Magmatic Evolution of the Western Myanmar Arc Documented by U-Pb and Hf Isotopes in Detrital Zircon. *Tectonophysics*, 612–613(3): 97–105. https://doi.org/10.1016/j.tecto.2013.11.039

Wen, D. R., Liu, D., Chung, S. L., et al., 2008. Zircon SHRIMP U-Pb Ages of the Gangdese Batholith and Implications for Neotethyan Subduction in Southern Tibet. *Chemical Geology*, 252(3/4): 191–201. https://doi.org/10.1016/j.chemgeo.2008.03.003

Wiedenbeck, M., Allé, P., Corfu, F., et al., 1995. Three Natural Zircon

Standards for U-Th-Pb, Lu-Hf, Trace Element and REE Analysis. *Geostandards and Geoanalytical Research*, 19(1): 1–23. https://doi.org/10.1111/j.1751-908X.1995.tb00147.x

Wörner, G., Moorbath, S., Harmon, R. S., 1992. Andean Cenozoic Volcanic Centers Reflect Basement Isotopic Domains. *Geology*, 20(12): 1103–1106. https://doi.org/10.1130/0091-7613(1992)020<1103:ACVCRB>2.3.CO;2

Xu, Y. G., Yang, Q. J., Lan, J. B., et al., 2012. Temporal-Spatial Distribution and Tectonic Implications of the Batholiths in the Gaoligong-Tengliang-Yingjiang Area, Western Yunnan: Constraints from Zircon U-Pb Ages and Hf Isotopes. *Journal of Asian Earth Sciences*, 53: 151–175. https://doi.org/10.1016/j.jseaes.2011.06.018

Yang, Q. J., Xu, Y. G., Huang, X. L., 2006. Geochronology and Geochemistry of Granites in the Gaoligong Tectonic Belt and Their Tectonic Implications. *Acta Petrologica Sinica*, 22(4): 817–834 (in Chinese with English Abstract)

Yang, Y. H, Wu, F. Y, Xie, L. W., et al., 2011. High-Precision Measurements of the $^{(143)}Nd/^{(144)}Nd$ Isotope Ratio in Certified Reference Materials without Nd and Sm Separation by Multiple Collector Inductively Coupled Plasma Mass Spectrometry. *Analytical Letters*, 43(1): 142–150. https://doi.org/10.1080/00032710903276539

Yonemura, K., Osanai, Y., Nakano, N., et al., 2013. EPMA U-Th-Pb Monazite Dating of Metamorphic Rocks from the Mogok Metamorphic Belt, Central Myanmar. *Journal of Mineralogical and Petrological Sciences*, 108(3): 184–188. https://doi.org/10.2465/jmps.121019a

Zaw, K., Meffre, S., Lai, C. K., et al., 2014. Tectonics and Metallogeny of Mainland Southeast Asia—A Review and Contribution. *Gondwana Research*, 26(1): 5–30. https://doi.org/10.1016/j.gr.2013.10.010

Zhu, D. C., Mo, X. X., Niu, Y. L., et al., 2009a. Geochemical Investigation of Early Cretaceous Igneous Rocks along an East-West Traverse throughout the Central Lhasa Terrane, Tibet. *Chemical Geology*, 268(3/4): 298–312. https://doi.org/10.1016/j.chemgeo.2009.09.008

Zhu, D. C., Mo, X. X., Wang, L. Q., et al., 2009b. Petrogenesis of Highly Fractionated I-Type Granites in the Zayu Area of Eastern Gangdese, Tibet: Constraints from Zircon U-Pb Geochronology, Geochemistry and Sr-Nd-Hf Isotopes. *Science in China Series D*: *Earth Sciences*, 52(9): 1223–1239. https://doi.org/10.1007/s11430-009-0132-x

Zhu, D. C., Zhao, Z. D., Niu, Y. L., 2011. The Lhasa Terrane: Record of a Microcontinent and Its Histories of Drift and Growth. *Earth and Planetary Science Letters*, 301(1–2): 241–255. https://doi.org/10.1016/j.epsl.2010.11.005